修士論文

FDTD-Q Analyses of a Mott Insulator Quantum Phase

モット絶縁体状態のFDTD-Q解析

平成19年2月2日

指導教員　山本 喜久 教授

東京大学大学院 情報理工学系研究科
電子情報学専攻 56434

藤原　史隆

FDTD-Q Analyses of a Mott Insulator Quantum Phase

by

Fumitaka Fujiwara

A dissertation presented to
Department of Information and Communication Engineering,
Graduate School of Information Science and Technology,
The University of Tokyo

in partial fulfillment of the requirements for the degree of
Master of Information Science and Technology

Supervisor: Professor Yoshihisa Yamamoto

Abstract

Quantum many-body problems model the behavior caused by the interactions between particles in a many-body system interacting via quantum mechanics. One well-known example of a quantum many-body problem is the Mott transition. According to band theory, which ignores the interactions between electrons, many materials that should be conductors are in fact Mott insulators. These materials are prevented from conducting due to the repulsive interactions between electrons.

The Mott transition is described by the Hubbard model, which is a minimal model that takes into account of not only the quantum mechanical motion of electrons in a solid but also the repulsive interaction between electrons. The Hubbard model can also describe not only such quantum phase transitions but also magnetism and superconductivity. Despite this importance, the Hubbard model is mathematically difficult to solve. To analyse the quantum many-body system described by the Hubbard model, quantum simulations, which simulate a quantum system by mapping into another simpler one with controllable parameters, have recently attracted a lot of attention.

Recently, a quantum phase transition from a superfluid state to a Mott insulator state was experimentally observed by a quantum simulation using optical lattices. In this experiment, the macroscopic property of the Mott insulator was observed in the form of an interference pattern. However the microscopic property can only be known unless the wave function is calculated.

In this dissertation, the “FDTD-Q method” which is an application of the finite-difference time-domain (FDTD) method is introduced to solve the time-dependent Schrödinger equation. In this study, using the FDTD-Q method, the wave function of a two-particle two-site system is calculated and the calculation is also extended to a three-particle system in a three-site geometry. The properties of a Mott insulator phase were analysed using these results.

Dedicated to you,
our future pioneers...

Table of Contents

List of Figures

List of Tables

Chapter 1

Introduction

1.1 Background

1.1.1 Quantum Many-body Problem

The quantum many-body problem may be defined as the study of the behavior caused by the effects of interaction between particles in a many-body system interacting via quantum mechanics. By describing the microscopic behavior of each particle, the macroscopic properties of the system, which appear as cooperative phenomena of the particles, is predicted. However, due to the exponential increase of the Hilbert space of the system, it becomes difficult to solve the set of equations determined by quantum mechanics.

Examples of quantum many-body problems include polymer molecules and materials in a solid state. Exact solutions are impossible in almost all many-body problems. A simple and efficient approach for solving quantum many-body problems is to ignore some interactions within the system. This allows the problem to be reduced to a simpler model.

As an example of this, in solid state physics, the nearly free electron model is a model of the electron's behavior in solids that enables to understand the electronic property of crystalline materials. The nearly free electron approximation can describe many properties of the electrons. One of consequences of this theory is that it predicts the same number of electrons in each unit cell. If the number of electrons is odd, it is expected that there is an unpaired electron in each unit cell. This means that the valence band is not fully occupied and, therefore, the material should be a conductor.

As described above, solving particular quantum many-body problems using certain approximations has allowed the properties of various materials to be understood. However this is very rare in many quantum many-body problems and, as a consequence, their properties are still unknown.

1.1.2 Mott Insulator

The band theory of solids had been successful in the describing the electrical properties of materials. However, in 1937, J. H. de Boer and E. J. W. Verwey pointed out that a variety of transition metal oxides, e.g. MnO, FeO, CoO, Mn_3O_4, NiO, etc., which were expected to be conductors according to band theory were in fact insulators [1]. Specifically, since MnO and CoO have an odd number of electrons per unit cell, they should theoretically be insulators. N. F. Mott and R. Peierls conjectured that this abnormal property could be caused by electron-electron interactions which are not considered in the formulation of conventional band theory [2]. Such materials are called Mott insulators.

In 1949, Mott proposed a model for NiO as an insulator [3]. In this case, conduction could be understood by the following formula:

$$(\mathrm{Ni}^{2+}\mathrm{O}^{2-})_2 \rightarrow \mathrm{Ni}^{3+}\mathrm{O}^{2-} + \mathrm{Ni}^{1+}\mathrm{O}^{2-} \tag{1.1}$$

The formation of the energy gap preventing conduction can be regarded as a competition between the Coulomb potential U between $3d$-electrons and the kinetic integral t of $3d$-electrons between neighbor-

ing atoms. Then, the total energy gap is

$$E_{\rm gap} = U - 2zt \tag{1.2}$$

where z is the number of the nearest neighbor atoms.

Generally, Mott insulators occur when the repulsive Coulomb potential U is large enough so that an energy gap arises. One of the simplest theories characterizing Mott insulators is the Hubbard model, which is referred to below.

1.1.3 The Hubbard Model

The Hubbard model is a model for electrons in a solid which strongly interact with each other through an extremely short-range repulsive Coulomb interaction [4]. The Hubbard model is a minimal model that takes into account for not only the quantum mechanical motion of electrons in a solid but also the repulsive interaction between electrons. In spite of its simplicity, it is thought to be a qualitative description of the properties of most solids. It is believed that the Hubbard model exhibits a variety of nontrivial phenomena, for example metal-insulator transitions, antiferromagnetism, ferrimagnetism, ferromagnetism, Tomonaga-Luttinger liquids, and superconductivity [5–8].

The Hamiltonian of the Hubbard model is made up with two parts:$H_{\rm hop}$ which represents the quantum mechanical hopping, and $H_{\rm int}$ which represents the repulsive interaction between electrons. Either $H_{\rm hop}$ and $H_{\rm int}$ alone is easily analyzed and the results can be easily interpreted. It is found that electrons behave as "waves" in $H_{\rm hop}$ and that, on the other hand, they behave as "particles" in $H_{\rm int}$. The problem becomes nontrivial when we consider electrons in a system with the Hamiltonian that is a sum of the two Hamiltonians ($H = H_{\rm hop} + H_{\rm int}$). This is related to the wave-particle dualism in quantum physics, which makes it a fascinating problem form the point of view of quantum mechanics.

The Hubbard model was originally proposed to describe electrons in solids and since has been considered as a model for high-temperature superconductivity. More recently, the the bosonic version of the model has been also studied [9] and has been used to describe the behavior of ultracold atoms trapped in optical lattices [12]. The model used for bosons is referred to as the "Bose-Hubbard model". In the following, I will explicitly write "Hubbard model" for the model of the electrons (or other fermions) and "Bose-Hubbard model" for the model of bosons.

From a mathematical point of view, the Hamiltonians $H_{\rm hop}$ and $H_{\rm int}$ do not commute with each other. Although each Hamiltonian can be easily diagonalized, it is nontrivial to analyze the property of their sum. However, one can get various interesting "physics" if one considers the problem of the competition between the wave-like nature and the particle-like nature. Consequently, to understand this problem is a very challenging issue and the model (in two dimensions) has remained unsolved for over fifty years.

1.1.4 Quantum Simulation

A universal quantum simulator was proposed by Richard P. Feynman in 1982 [14]. Feynman showed that a classical Turing machine takes exponentially increasing time with the problem size when simulating quantum many-body systems exactly, whereas his hypothetical quantum simulator would not. In a quantum simulator, the quantum system is recreated in another simpler quantum system with controllable parameters. Such simulation is called quantum simulation.

In a real material, a parameter can be modified only within a small range, so that the information gained by experiments is rather limited. However a quantum simulator is easier to implement compared to a universal quantum computer owing to no need for local control operation and isolation from external reservoirs. Consequently, a quantum many-body system is able to be simulated over a wide parameter range.

Recently, quantum simulations of the Hubbard model and the Bose-Hubbard model have been implemented and studied about quantum phase transitions. Through these experiments performed with quantum simulators, phenomena which are impossible to calculate theoretically due to their complexity might be revealed.

1.2 Objectives

1.2.1 Quantum Phase Transition in a Gas of Ultracold Atoms

For a system at absolute zero temperature, all thermal fluctuations vanish, while quantum fluctuations remain. These microscopic quantum fluctuations can produce a macroscopic phase transition in the ground state of a many-body system when either the interaction energy between particles overcomes the kinetic energy, or vice versa.

In 2002, a quantum phase transition was observed in a system consisting of a Bose-Einstein condensate of ^{87}Rb atoms with repulsive interactions, held in a three-dimensional optical lattice potential [17]. As the potential depth of the optical lattice increased, the quantum phase changes from a superfluid phase into a Mott insulator phase. In the superfluid state, each atom is delocalized throughout the entire lattice with long-range phase coherence. In contrast, the Mott insulator state has exact numbers of atoms localized at each lattice site without phase coherence.

In the experiment described above, the phase coherence between different lattice sites was tested by observing interference patterns of atoms after a sudden termination of the confining lattice potential. In the superfluid phase, where all atoms are spread out over the entire lattice with equal relative phases between different lattice sites, a high-contrast three-dimensional interference pattern was obtained as expected for a periodic array of phase coherent matter wave sources. On the other hand, in the Mott insulator phase, where atoms are tightly localized at a single lattice site with no phase coherence, no interference pattern was visible.

1.2.2 Necessity of Numerical Analysis

The existence of the Mott insulator was revealed by a true experiment where an interference pattern was observed. The interference pattern shows that each atom is localized at an individual site. However, although that experiment is interesting in itself, we can only deduce macroscopic properties of a many-body system which arises from the result of microscopic behavior of each atom. To know the true state of each particle, there is a need for the wave function of the system to be calculated.

Of course, it is computationally impossible to analyse the wave function of such a system with many particles. It is necessary to reduce the number of particles and to simplify the system for the numerical analysis. However, even if the system contains only two particles in two-site geometry, we can know the correlation between the two particles by the numerical simulation. Consequently, this simulation also would aid the understanding of the true nature of Mott insulators.

1.3 Description of the Remaining Chapters

The outline of this dissertation is as follows.

Chapter 2 contains the details of the Hubbard model and quantum simulations. Examples of quantum simulators for both the Hubbard model and the Bose-Hubbard model are introduced. In this chapter, I will explain the difference between the superfluid phase and the Mott insulator phase in detail. I will then comment on the necessity of numerical analysis of the Mott insulator state.

Chapter 3 contains numerical methods for solving the time-dependent Schrödinger equation. The "FDTD-Q method" is introduced, which is a modification of the FDTD method widely used for solving Maxwell's equations. Conditions for the calculations are also described in this chapter.

Chapter 4 contains the implementation of the FDTD-Q simulations of a two-particle system in a two-site geometry. The general outline of numerical simulation is described and results of the simulation are also seen in this chapter.

Chapter 5 contains the implementation of the FDTD-Q simulations of a three-particle system in a three-site geometry. In this chapter, the numerical simulation is extended to a three-particle system for the generality.

Chapter 6 contains the conclusions of this dissertation. In addition, future prospects are also described.

Chapter 2

Quantum Simulations of the Hubbard Model

2.1 The Hubbard Model

2.1.1 Overview

The Hubbard model is an approximate model used in solid state physics to represent quantum phase transitions between conducting and insulating states. The Hubbard model is the simplest model of interacting particles in a lattice, containing only two terms in Hamiltonian: kinetic and potential terms [4]. The kinetic term allows tunneling, or hopping, of particles between sites of the lattice. The potential term consists of on-site interactions.

Although, the standard Hubbard model considers electrons, the particles can also be any type of fermion. In addition, the model has been extended to bosons in the form of the Bose-Hubbard model [9].

The Hubbard model is mainly based on the tight-binding approximation in solid state physics. In the tight-binding approximation, electrons are considered to occupy the standard orbits of their constituent atoms. These electrons hop between atoms during conduction. Mathematically, this is represented as a hopping integral or a transfer integral between nearby atoms, which can be considered as the physical principle that creates electron bands in crystalline materials. However, in this approximation, interactions between electrons are ignored .

By formulating conduction in terms of a hopping integral, the Hubbard model also contains the on-site repulsions originating from the Coulomb repulsive interactions between electrons. This involves competition between the hopping integral, which moves electrons between neighboring atoms, and the on-site repulsive interaction, which does not. In this way, the Hubbard model can explain Mott insulators, which are prevented from becoming conducting by the strong repulsive interactions between particles.

2.1.2 Definition of the Hubbard Model

Let the lattice Λ be a collection of sites $x, y, \ldots$. In the Hubbard model, each lattice site corresponds to an atomic site in a crystal. In order to simplify the situation significantly, it is assumed that each atom has only one electron orbit and the corresponding orbital state is non-degenerate. Because electrons in other states do not play important roles in determining the low-energy physics, they can be ignored (See Fig.2.1).

Field Operators

Here, x is a position of the electron in the lattice sites Λ, and σ is a spin of the electron which can be up ($\uparrow$) or down ($\downarrow$). $c^\dagger_{x,\sigma}$ is the fermion creation operator, which creates an electron with spin σ at site x, and $c_{x,\sigma}$ is the fermion annihilation operator, which annihilates an electron with spin σ at site x. $n_{x,\sigma} = c^\dagger_{x,\sigma} c_{x,\sigma}$ is the number operator. These fermion operators obey the canonical anti-commutation relations

$$\{c^\dagger_{x,\sigma}, c_{y,\tau}\} = c^\dagger_{x,\sigma} c_{y,\tau} + c_{y,\tau} c^\dagger_{x,\sigma} = \delta_{x,y}\delta_{\sigma,\tau} \tag{2.1}$$

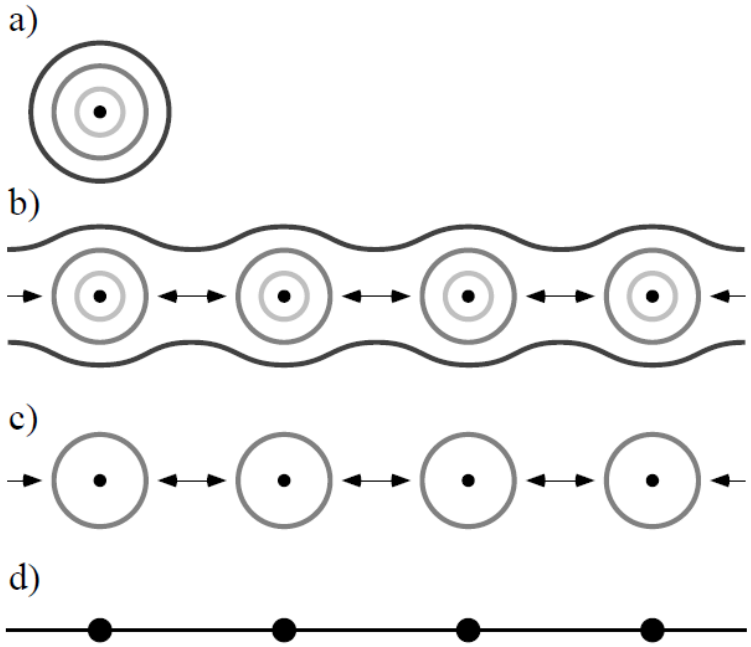

Fig. 2.1: A Highly Schematic View of Tight-binding Descriptions. a) a single atom with multiple electrons in different orbits. b) In a solid, electrons in the black orbits can move around, while those in the light gray orbits are localized at the original atomic sites. The electrons in the gray orbits are mostly localized around the atomic sites, but there is a non-negligible tunneling probability of hopping to nearby gray orbits. c) Electrons only in gray orbits are considered, which are expected to play an essential role in determining the properties of the system. d) Assuming that the gray orbit is non-degenerate, a lattice model that electrons stay on lattice sites and hop from a site to another is obtained.

and

$$\{c^\dagger_{x,\sigma}, c^\dagger_{y,\tau}\} = c^\dagger_{x,\sigma}c^\dagger_{y,\tau} + c^\dagger_{y,\tau}c^\dagger_{x,\sigma} = 0, \tag{2.2}$$

where $\delta_{i,j}$ is the Kronecker delta.

The state without any electrons is represented as $|\Psi_{\rm vac}\rangle$, defined by the following equation

$$c_{x,\sigma}|\Psi_{\rm vac}\rangle = 0 \qquad (\,\forall x, \sigma\,). \tag{2.3}$$

The Hilbert space of the model is generated by the states derived by multiplying the creation operator $c^\dagger_{x,\sigma}$ with various x and σ onto the state $|\Psi_{\rm vac}\rangle$. Because the anti-commutation relation (Eq. (2.2)) implies

$$(c^\dagger_{x,\sigma})^2 = 0, \tag{2.4}$$

the state of each lattice site can be either vacant, occupied by a single electron with a spin $\uparrow$ or $\downarrow$, or occupied by two electrons with spins both $\uparrow$ and $\downarrow$. Since four states exist par a lattice site, the total dimension of the Hilbert space is $4^{|\Lambda|}$, where $|\Lambda|$ is the number of lattice sites.

Hamiltonian

The Hamiltonian of the Hubbard model is represented as the sum of two elements

$$H = H_{\mathrm{hop}} + H_{\mathrm{int}}. \tag{2.5}$$

The hopping Hamiltonian H_{hop} generally has the form

$$H_{\mathrm{hop}} = \sum_{x,y\in\Lambda} \sum_{\sigma=\uparrow,\downarrow} t_{x,y} c^{\dagger}_{x,\sigma} c_{y,\sigma}. \tag{2.6}$$

The hopping amplitude $t_{x,y} = t_{y,x}$, assumed to be real, describes the quantum mechanical amplitude for an electron to hop from site x to y (or from y to x). When $x = y$, that is an electron stays at the present lattice site, the summand of Eq. (2.6) becomes

$$t_{x,x} c^{\dagger}_{x,\sigma} c_{x,\sigma} = t_{x,x} n_{x,\sigma}, \tag{2.7}$$

which is simply a single-body potential at the site x.

On the other hand, the interaction Hamiltonian H_{int} is generally written

$$H_{\mathrm{int}} = \sum_{x\in\Lambda} U_x n_{x,\uparrow} n_{x,\downarrow}. \tag{2.8}$$

Often U_x is set to be a constant ($U_x = U$). For $U_x > 0$, Hamiltonian corresponds to repulsive interaction. When two electrons occupy a single site at x, the total energy of the system rises by U_x. Although the original Coulomb interaction is long ranged, only on-site short-range interactions are taken into account as the main and strongest part of the interaction. This equation can also be interpreted such that the long-range part of the Coulomb interaction is screened by the electrons in different orbital states which are ignored in the Hubbard model.

Total Number Operator

The total number operator is defined as

$$\hat{N}_e = \sum_{x\in\Lambda} (n_{x,\uparrow} + n_{x,\downarrow}). \tag{2.9}$$

This operator commutes with the Hamiltonian H. $\hat{N}_{\mathrm{e}}$ is a conserved quantity, such as the total spin. Stationary states of the system are obtained by keeping the eigenvalue $\hat{N}_{\mathrm{e}}$ constant. In the following, only the Hilbert space with the number operator $\hat{N}_{\mathrm{e}}$ having a fixed eigenvalue N_{e} is considered. Since every lattice site can have at most two electrons, N_{e} satisfies

$$0 \leq N_{\mathrm{e}} \leq 2|\Lambda|. \tag{2.10}$$

The total electron number N_{e} is one of the most fundamental parameters in the Hubbard model.

2.1.3 Extreme Situations of the Hubbard Model

In order to comprehend the sum of the two Hamiltonians in the Hubbard model, two limits are discussed here.

Non-interacting System

Let us assume that the repulsive Coulomb interaction in $H_{\rm int}$ satisfies

$$U_x = 0 \qquad (\ \forall x \in \Lambda\ ). \tag{2.11}$$

The Hamiltonian is then

$$H = H_{\rm hop} = \sum_{x,y\in\Lambda}\sum_{\sigma=\uparrow,\downarrow} t_{x,y} c^\dagger_{x,\sigma} c_{y,\sigma}. \tag{2.12}$$

Since Eq. (2.12) is quadratic in fermion operators, it can be diagonalized easily. The single-electron Schrödinger equation corresponding to the hopping Hamiltonian $H_{\rm hop}$ is

$$\sum_{y\in\Lambda} t_{x,y}|\phi_y\rangle = \varepsilon|\phi_x\rangle, \tag{2.13}$$

where $|\boldsymbol{\phi}\rangle = (|\phi_x\rangle)_{x\in\Lambda}$ is a wave function of the single-electron, and ε is the single-electron energy eigenvalue. The eigenvalue and eigenstates of Eq. (2.13) are respectively denoted as ε_j and $|\boldsymbol{\phi}^{(j)}\rangle = (|\phi^{(j)}_x\rangle)_{x\in\Lambda}$, with the index $j = 1, 2, \ldots, |\Lambda|$. The energy levels are ordered as $\varepsilon_j \le \varepsilon_{j+1}$ with considering degeneracies.

Let us now consider a simple example. Consider a one-dimensional lattice $\Lambda = 1, 2, \ldots, N$ and impose periodic boundary conditions, that is, the site $x + N$ is identified as the site x. As for the hopping matrix elements, I assume that following values:

$$\begin{cases} t_{x,x+1} = t_{x+1,x} = -t & (\ \forall x \in \Lambda\ ) \\ t_{x,y} = 0 & (\ \text{otherwise}\ ) \end{cases}. \tag{2.14}$$

The corresponding Schrödinger equation (2.13) can be easily solved according to the wave function $\frac{1}{\sqrt{N}}e^{ikx}$, with wave number

$$k = \frac{2\pi n}{N} \qquad (\ n = 0, \pm1, \pm2, \ldots, \pm\frac{N}{2}\ ). \tag{2.15}$$

The eigenvalues are $\varepsilon(k) = -2t\cos k$. If one makes a suitable correspondence between n and $j = 1, 2, \ldots, N$, the desired energy level ε_j is obtained.

Now let us define the fermion operators corresponding to the eigenstates $|\boldsymbol{\phi}^{(j)}\rangle$ by

$$a^\dagger_{k,\sigma} = \sum_{x\in\Lambda} c^\dagger_{x,\sigma}\frac{1}{\sqrt{N}}e^{ikx}. \tag{2.16}$$

Due to the orthonormality of the set of eigenstates $\{|\boldsymbol{\phi}^{(j)}\rangle\}_{j=1,2,\ldots,|\Lambda|}$, one finds that the inverse transformation of Eq. (2.16) is

$$c^\dagger_{x,\sigma} = \sum_{k=-\pi,-\pi+\frac{2\pi}{N},\ldots,\pi} a^\dagger_{k,\sigma} e^{-ikx}. \tag{2.17}$$

Substituting Eq. (2.17) into Eq. (2.6) and using Eq. (2.13), $H_{\rm hop}$ can be diagonalized as

$$H_{\rm hop} = \sum_{\sigma=\uparrow,\downarrow}\sum_k \varepsilon(k) a^\dagger_{k,\sigma} a_{k,\sigma} = \sum_{\sigma=\uparrow,\downarrow}\sum_k \varepsilon(k)\tilde{n}_{k,\sigma}, \tag{2.18}$$

where $\tilde{n}_{k,\sigma} = a^\dagger_{k,\sigma} a_{k,\sigma}$ can be interpreted as the electron number operator for the eigenstate with momentum k.

Here, let A and B be arbitrary subsets of $\{-\pi, -\pi + \frac{2\pi}{N}, \ldots, \pi\}$ which satisfy $|A| + |B| = N_{\mathrm{e}}$. By using Eq. (2.18), the state

$$|\Psi_{A,B}\rangle = \left(\prod_{k \in A} a^{\dagger}_{k,\uparrow} \right) \left(\prod_{k \in A} a^{\dagger}_{k,\downarrow} \right) |\Psi_{\mathrm{vac}}\rangle \tag{2.19}$$

is found to be an eigenstate of $H = H_{\mathrm{hop}}$ and its energy eigenvalue is

$$E_{A,B} = \sum_{k \in A} \varepsilon(k) + \sum_{k \in B} \varepsilon(k). \tag{2.20}$$

The ground state of this non-interacting system can be obtained by choosing subsets A and B which minimize the energy $E_{A,B}$.

When the corresponding single-electron energy eigenvalues are non-degenerate, i.e. $\varepsilon_j < \varepsilon_{j+1}$, and the total electron number N_{e} is even, the ground state of the system with the Hamiltonian $H = H_{\mathrm{hop}}$ is written

$$|\Psi_{\mathrm{GS}}\rangle = \left(\prod_{j=1}^{N_{\mathrm{e}}/2} a^{\dagger}_{k(j),\uparrow} a^{\dagger}_{k(j),\downarrow} \right) |\Psi_{\mathrm{vac}}\rangle. \tag{2.21}$$

This indicates that the state is filled with both up and down spins from the lowest energy level. See Fig. 2.2.

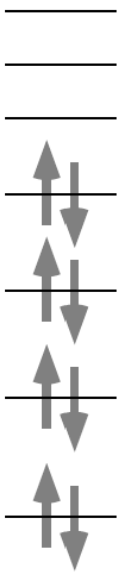

Fig. 2.2: The Ground State of a Non-interacting System. The lowest $\frac{N_{\mathrm{e}}}{2}$ energy levels of a single electron system are filled with up and down spin electrons.

In the discussion above, the electron has a plane wave form with a certain wave number k. The diagonalization of the Hamiltonian $H = H_{\mathrm{hop}}$ shows that the electrons behave as "waves" in this non-interacting system.

Non-hopping System

Let us now assume that the hopping matrix elements in $H_{\rm hop}$ satisfy

$$t_{x,y} = 0 \qquad (\ \forall x, y \in \Lambda\ ). \tag{2.22}$$

The Hamiltonian is then

$$H = H_{\rm int} = \sum_{x\in\Lambda} U_x n_{x,\uparrow} n_{x,\downarrow}, \tag{2.23}$$

which is in fact already diagonalized. A general eigenstate can be written

$$|\Psi_{X,Y}\rangle = \left(\prod_{x\in X} c^\dagger_{x,\uparrow}\right)\left(\prod_{y\in Y} c^\dagger_{y,\uparrow}\right)|\Psi_{\rm ac}\rangle, \tag{2.24}$$

where X and Y are arbitrary subsets of Λ, and represent lattice sites which are occupied by up and down spin electrons. The total electron number in this state is given by

$$N_{\rm e} = |X| + |Y|, \tag{2.25}$$

and the energy eigenvalue is given by

$$E_{X,Y} = \sum_{x\in X\cap Y} U_x. \tag{2.26}$$

For a given electron number $N_{\rm e}$, the ground state can be found by choosing subsets X and Y that minimize the energy $E_{X,Y}$. In the case of $N_{\rm e} \leq |\Lambda|$, if the subsets X and Y are chosen as satisfying $X \cap Y = \emptyset$, i.e. two electrons do not exist on a same site. The energy of the ground state then equals to 0.

Needless to say, the electrons behave as "particles" in this non-hopping system, which repulsively interact only when two happen to be on a same site.

2.1.4 Expansion into the Bose-Hubbard Model

The Bose-Hubbard model is an approximate model of interacting bosons on a lattice. It is closely related to the Hubbard model which originated from solid state physics as an approximate representation of the behavior of the electrons confined in atomic potentials of a crystalline solid. The difference is that the fermionic operators are now replaced by bosonic creation and annihilation operators. The Bose-Hubbard model is used to study systems such as bosonic atoms in optical lattices.

The Hamiltonian of the Bose-Hubbard model is given by

$$H = -t \sum_{\{(x,y)|\text{nearest neighbor}\}} (b^\dagger_x b_y + b^\dagger_y b_x) + \frac{1}{2}U\sum_x \hat{n}_x(\hat{n}_x - 1) - \sum_x \mu_x \hat{n}_x, \tag{2.27}$$

where $b^\dagger_x$ and b_x are bosonic creation and annihilation operators, satisfying

$$[b_x, b^\dagger_y] = \delta_{x,y} \tag{2.28}$$

and

$$[b_x, b_y] = 0. \tag{2.29}$$

$\hat{n}_x = b_x^\dagger b_x$ is the number operator and it gives the number of the particles at the site x. t is the hopping matrix element, U is the on-site interaction, and μ_x is the chemical potential.

In fermionic systems, the Mott transition are complicated due to the spin of electrons and the anti-commutating nature of the operators. On the other hand, for interacting bosonic system with spin zero, the situation is much simpler and more easily studied. Therefore theoretical analyses of the dynamics of the Bose-Hubbard model are often studied [10, 11].

2.2 Quantum Phase Transition

2.2.1 Overview

Due to Heisenberg's uncertainty, fluctuations remain even at zero temperature in a quantum system. These quantum fluctuations may be strong enough to induce a quantum phase transition which brings about a macroscopic change. A remarkable example of such a quantum phase transition is the shift from the superfluid state to the Mott insulator state in a system made up of bosonic particles which repulsively interact each other. This transition was first studied theoretically [9] and, recently, have been shown to be observable when an ultracold gas of atoms with repulsive interactions is stored in a periodic potential [12].

Let us consider an atomic gas of bosons at extremely low temperatures. In such an ultracold situation, a Bose-Einstein condensate is formed. When a lattice potential is applied on the Bose-Einstein condensate, this results in a superfluid state with long-range phase coherence. In the superfluid state, bosons can hop from one lattice site to the next only by a tunnel coupling.

If the lattice potential is raised smoothly, the system stays in the superfluid state as long as atom-atom interactions are small relative to the tunnel coupling. In this phase, the delocalized wave function minimizes the kinetic energy which is dominant in the system and therefore the total energy is also minimized.

If the lattice potential is raised further, the repulsive atom-atom interactions become large compared to the tunnel coupling. In this phase, since the total energy is minimized when each lattice site is filled with the same number of atoms, the atom number per site becomes fixed. This is accompanied by the reduction of fluctuations in the atom number on each site, and phase coherence is consequently lost. This situation is called the Mott insulator phase.

The above physics can be described by the Bose-Hubbard model (see Eq. (2.27)). In the following, the two main phases of the model, i.e. the superfluid state and the Mott insulator state, is discussed.

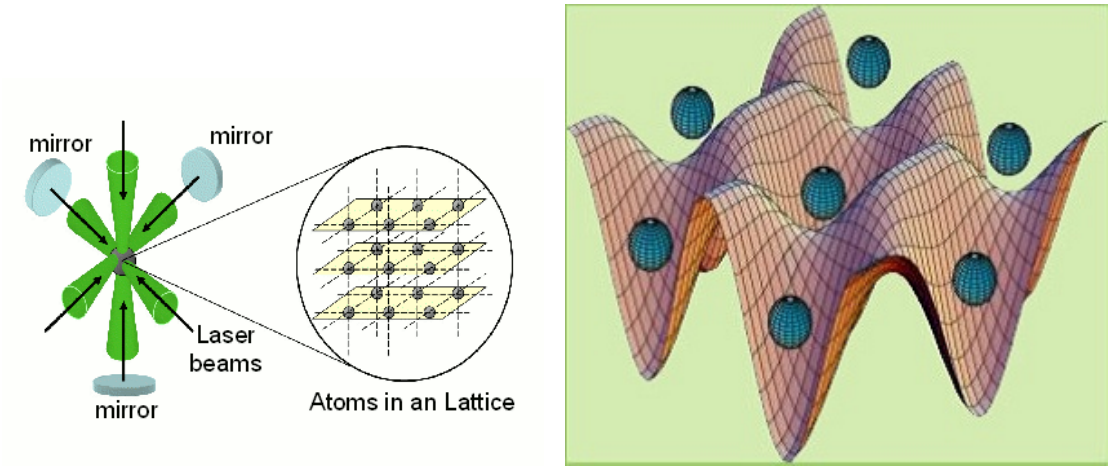

(a) Optical Lattices (b) Lattice Potential

Fig. 2.3: Ultracold Atoms in Optical Lattices

2.2.2 Superfluid Phase

In the limit where the tunneling (hopping) term dominates the Hamiltonian, the total energy of the ground state is minimized by single-particle wave functions that are spread out over the entire lattice. The many-body ground state for a homogeneous system ($\mu_x = \text{constant}$) is given by

$$|\Psi_{\text{SF}}\rangle_{U=0} \propto \left(\sum_{x=1}^{M} a_x^\dagger \right)^N |\Psi_{\text{vac}}\rangle, \tag{2.30}$$

where M is the lattice site number, and N is the atom number. Note that this is equivalent to the plane wave states discussed in Subsection 2.1.3, with all $k = 0$.

In this regime, all atoms occupy identical extended Bloch states. Furthermore this regime is well represented by a macroscopic wave function with long-range phase coherence over the entire lattice.

2.2.3 Mott Insulator Phase

In the opposite limit, where the interaction term dominates the Hamiltonian, the ground state of the system consists of wave functions of localized atoms with a same number per site. Then the ground state is a product of local Fock states for each lattice site. The many-body ground state for a filling factor n (n atoms per site) is given by

$$|\Psi_{\text{MI}}\rangle_{t=0} \propto \left(\prod_{x=1}^{M} (a_x^\dagger)^n \right) |\Psi_{\text{vac}}\rangle, \tag{2.31}$$

in the homogeneous case.

This Mott insulator state cannot be expressed by a macroscopic wave function. In this regime, no phase coherent prevails in the system but there exists perfect correlations in the atom number between lattice sites.

2.3 Quantum Simulation

2.3.1 Universal Quantum Simulator

In 1982, Richard Feynman proposed that a universal quantum computer could be used to simulate physical systems [14]. Since the number of variables that must be taken into account to simulate a quantum system increases exponentially with the number of particles in the system, he claimed that the simulations of quantum many-body systems are intractable on any classical computer, and conjectured that other computers built incorporating quantum mechanics should be able to simulate quantum mechanical systems efficiently. It is known that certain phenomena in quantum field theory are well imitated by certain condensed matter systems and therefore he guessed that there should be a certain class of quantum systems which would simulate any other systems, a so-called "Universal Quantum Simulator".

In 1996, Seth Lloyd showed Feynman's conjecture to be correct [15]. Furthermore, he also indicated that the experimental requirements to accomplish an efficient simulation of interacting many-body systems would be less demanding compared to the implementation of Shor's factoring algorithm [16], which is the best known problem that a quantum computer can solve more efficiently than a classical computer. Although a quantum computer implementing Shor's algorithm might need millions of quantum bits (qubits), quantum simulation requires a quantum computer (simulator) with only a few hundreds or thousands qubits.

2.3.2 Benefits of Quantum Simulations

With quantum simulators, many condensed matter phenomena described by a many-body Hamiltonian that cannot be treated either analytically or numerically with classical computers, are thought to become tractable. Therefore, through these experiments, important phenomena in physics, chemistry, and even biology are hoped to be understood.

The experiment of ultracold atoms stored in optical lattices is the most successful implementation of a quantum simulator to date. The lattices are artificial crystals made of laser light (Fig. 2.3(a)) where ultracold atoms are confined in arrays of a microscopic potential (Fig. 2.3(b)). They can be manipulated externally by optical techniques. Due to the many controllable parameters over the atoms, this system is highly suited for performing quantum simulations.

2.4 Quantum simulation of the Hubbard Model

Recently there have been a lot of advances in trapping of fermionic atoms in optical lattices [18]. One of the features of an optical lattice is that the effective form of interactions is an extremely short-range

interaction [13]. In a real system where the physics is described by a Hubbard model, the interactions are of a long-range form originating from the Coulomb interaction. Therefore such effects may be difficult to take into account in an optical lattice approach. To simulate a Coulomb interaction, a real Coulomb interaction may be necessary in the system carrying out the simulation.

2.4.1 Quantum Simulator Using Surface Acoustic Waves

Another type of quantum simulator using fermionic particles were proposed for studying the Hubbard model [19]. This quantum simulator is desired to understand the metal-Mott insulator (conducting-insulating) quantum phase transition in a solid.

In Ref. [19], Byrnes et al. start with a standard modulation-doped GaAs/AlGaAs heterojunction, which forms a two-dimensional electron gas (2DEG). Interdigital transducers (IDTs) are placed outside of the 2DEG mesa. Surface acoustic waves (SAWs) are launched by driving a high frequency AC voltage to the IDTs, forming an interference area at the center of the device. An electric potential is induced due to the piezoelectric property of GaAs. As the SAW moves, it carries the trapped electron with it in the local minima of the potential induced by the SAW [20]. The electrons in the lattice interact via a Coulomb repulsive force and thus create a Hubbard model (see Fig. 2.4).

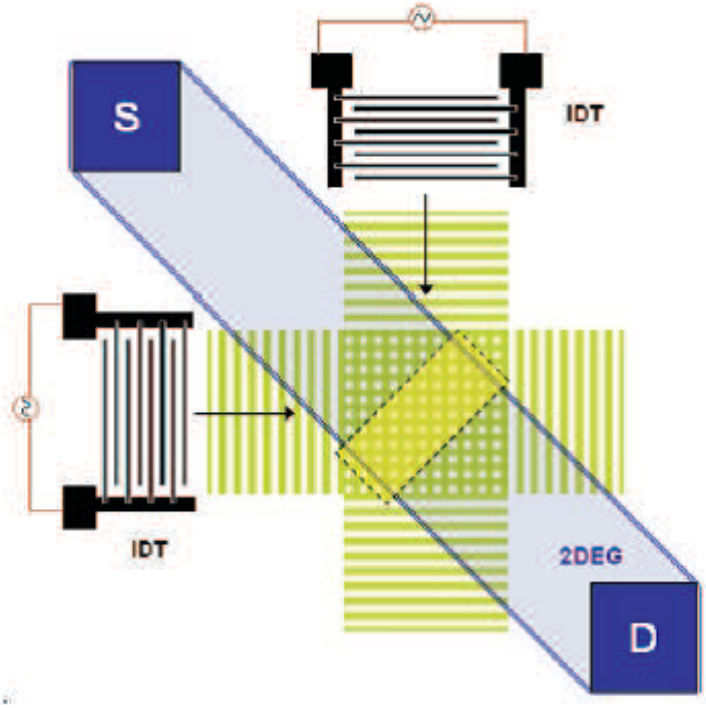

Fig. 2.4: Quantum Simulator Using SAW. Green areas show periodic potential experienced by electrons. “S” denotes a source electrode and “D” a drain electrode.

2.5 Quantum Simulation of the Bose-Hubbard Model

In 2002, Markus Greiner et al. observed a quantum phase transition in a Bose-Einstein condensate of ^{87}Rb, held in a three-dimensional optical lattice potential [17]. In this experiment, the phase coherence between different lattice sites was tested by suddenly turning off the confining potential. The atoms were then permitted to expand freely and interfere with each other.

2.5.1 Superfluid Phase

In the superfluid phase, where all atoms are delocalized throughout the entire lattice with equal relative phases between different lattice sites, a high-contrast three-dimensional interference was detected as expected for a periodic array of phase coherent matter wave source (Fig. 2.5).

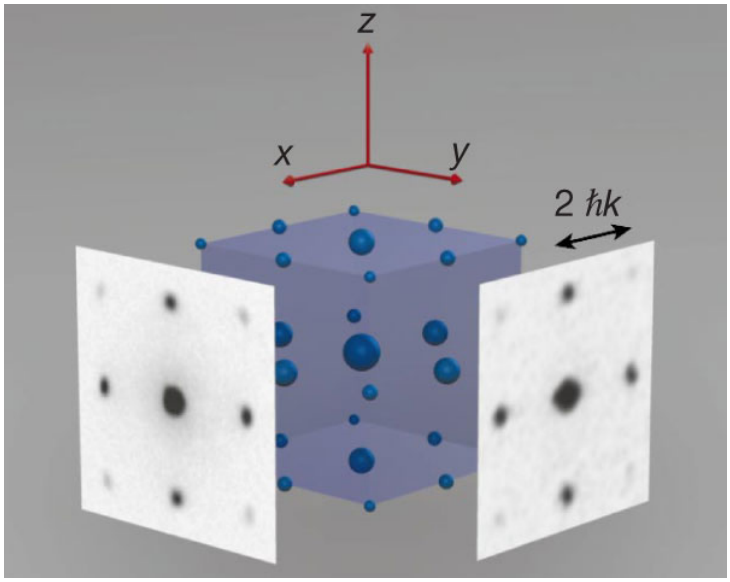

Fig. 2.5: Schematic Three-dimensional Interference Pattern. k denotes the wave vector of the laser light. (Excerpted from Ref. [17])

2.5.2 Quantum Phase Transition into the Mott Insulator Phase

As the lattice potential height is increased, the resulting interference pattern changes markedly. In the initial state, where there exists no lattice potential, the Bose-Einstein condensate has perfect phase coherence and therefore only a first-order interference peak is observed (Fig. 2.6a). The strength of higher-order interference maxima increases as the lattice depth is increased because the atoms tightly localize on every lattice site (Figs. 2.6b-d). When the lattice potential is further increased, the strength of the interference maxima no longer increases (Figs. 2.6e, f). Instead, an incoherent background appears. Finally, no interference pattern is visible at all (Figs. 2.6 g, h). Phase coherence has been absolutely lost at this lattice potential.

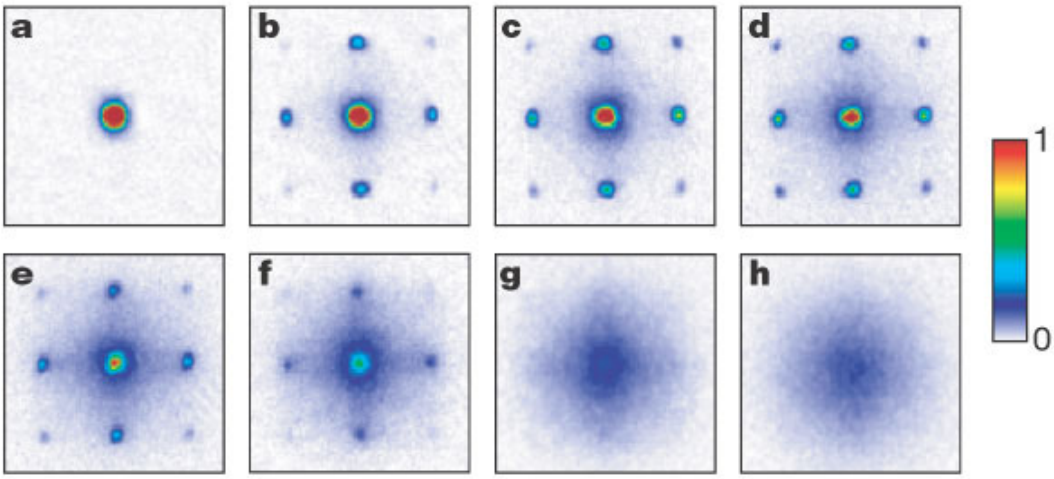

Fig. 2.6: Absorption Images of Multiple Matter Wave Interference Patterns. These were obtained after suddenly releasing the atoms from an optical lattice potential with different potential depths. (Excerpted from Ref. [17])

During the evolution, the interference pattern remarkably changes from the coherent to the incoherent. When the interference pattern is still visible, no broadening of the interference maxima can be observed. With a strong lattice potential, this completely vanishes in the incoherent background. This phenomenon can be explained on the basis of the superfluid-Mott insulator phase diagram. After the system has crossed over the quantum critical point, it changes into an incoherent Mott insulator phase. Near this quantum critical point, the system is inhomogeneous, that is to say, partially in the superfluid state and also partially in the Mott insulator state. Therefore both interference peaks and incoherent background are visible.

2.6 Problems and Requirements

Ultracold atoms in optical lattices have experimentally realized a Mott insulator state. The interference pattern indicates that each atom is localized at an individual site [17]. However the behavior of each particle in the Mott insulator state is unclear from this experiment alone. To understand the true behavior of each particle, the wave function of the quantum many-body system must be calculated.

Of course, it is impossible to calculate the wave function of such a system of tens or hundreds particles with computers. Thus it is necessary to reduce the particle number and simplify the system for numerical analysis. Even if the target system contains only two particles, one can know the correlation between the two particles using a numerical simulation. It is hoped to gain a better understanding of Mott insulators using this calculation.

Chapter 3

FDTD-Q method

3.1 Numerical Analysis

3.1.1 Numerical Solutions for Partial Differential Equations

Numerical schemes for solving partial differential equations, e.g. Maxwell's equations and the time-dependent Schrödinger equation, include the following:

- The finite difference method
  Functions are discretized and then represented by their values at certain grid points and derivatives are approximated through differences in these values. Finite differences are one of the simplest ways of approximating a differential operator.

- The finite element method
  Functions are represented in terms of basis functions and the partial differential equations are solved in their integral form. The solution is based on eliminating the differential equation completely, or rendering the partial differential equation into an equivalent ordinary differential equation with standard solutions.

- The finite volume method
  Space is divided into discrete parts and the change within each volume is calculated by considering the flux across the surface of each volume.

- The spectral method
  Functions are represented as a sum of their basis functions, for example Fourier components. By substituting the Fourier decompositions into the original partial differential equations, a system of ordinary differential equations is obtained.

The finite difference method is usually regarded as the simplest and the most easily understood method and thus we usually choose to use this finite difference method. The finite element and the finite volume methods are widely used in engineering and in computational fluid dynamics, and are suited for problems in complicated geometries. The spectral methods are generally the most accurate, if the solutions are sufficiently smooth.

In this chapter, the finite difference method is employed for solving the time-dependent Schrödinger equation. This scheme is adopted not only for the spatial domain but also for the temporal domain. Consequently, using this scheme, the time response of the wave function is calculated and the scattering of the quantum particle can be calculated.

3.1.2 Explicit Versus Implicit Schemes

For numerically solving partial differential equations, either explicit scheme or implicit scheme, as well as semi-implicit scheme, may be applied. Explicit methods calculate the state of a system at a later time, or a next time step, only from the state of the system at the current time. On the other hand, implicit methods find the later state by solving an equation involving both the current state of the system

and the later one. The explicit method is called as the "forward Euler method", while the implicit method is called as the "backward Euler method". Moreover the semi-implicit method is called the "Crank-Nicolson method". This method involves taking the derivative half way between the beginning and the end of the time step. It is thus an average between the fully implicit and fully explicit schemes.

The explicit method is stability bound, but much faster on a per-time-step basis. Furthermore, because the time step is severely restricted, this method tends to produce a more temporally accurate solution. Generally, the explicit method is suitable for time-dependent problems with fast moving dynamics.

The main advantage of the implicit approach is to march in large time steps for the steady state without any stability conditions. The price for stability is the need to solve a linear algebraic system at each demanding time step, which is a rather expensive computational task and therefore takes a lot of time. In addition, although harmless to stability, the time-step size has to be carefully chosen, due to the numerical accuracy of the time evolution.

3.1.3 Solutions of the Time-dependent Schrödinger Equation

The numerical solutions of the time-dependent Schrödinger equation (or similar equations) have been studied for a long time in order to calculate the dynamics of quantum mechanical systems [21–24]. These time-domain calculations are useful for estimating the response of various quantum devices. In the following sections, I introduce a solution for the time-dependent Schrödinger equation with a focus on the "FDTD-Q method".

3.2 The FDTD-Q Algorithm (Real Time)

The finite-difference time-domain (FDTD) is a computational electrodynamics modeling scheme. It is widely used to solve Maxwell's equations for scientific and engineering applications [26, 27].

The FDTD method belongs to the general class of grid-based differential time-domain numerical modeling methods. Maxwell's equations (in partial differential form) are transformed into central-difference equations. The equations are solved in a leapfrog manner: the electric field is solved at a given instant in time, then the magnetic field is solved at the next instant in time, and the process is iterated over and over.

This scheme is also useful for the analysis of quantum devices [28, 29]. The scheme is extended for solving the time-dependent Schrödinger equation

$$i\hbar\frac{\partial\psi(\boldsymbol{r},t)}{\partial t} = \hat{H}\psi(\boldsymbol{r},t), \tag{3.1}$$

where the Hamiltonian has the form

$$\hat{H} = -\frac{\hbar^2}{2m}\nabla^2 + V(\boldsymbol{r},t), \tag{3.2}$$

where m is the mass of the particle and V is the potential.

In this section, I will describe an application algorithm of the FDTD technique for solving the time-dependent Schrödinger equation. In the following, to distinguish the two algorithms, I call the scheme "FDTD" for electromagnetism and "FDTD-Q" for quantum mechanics.

3.2.1 Separation of Real and Imaginary Parts

To obtain two real equations, the complex wave function is separated into two real functions. They correspond to the real and imaginary parts

$$\psi(\boldsymbol{r},t) = \psi_{\rm re}(\boldsymbol{r},t) + i\psi_{\rm im}(\boldsymbol{r},t). \tag{3.3}$$

Then, by separating real and imaginary parts, Eq. (3.1) is divided into the following two equations involving real functions corresponding to $\psi_{\rm re}$ and $\psi_{\rm im}$.

$$\hbar\frac{\partial\psi_{\rm re}(\boldsymbol{r},t)}{\partial t} = -\frac{\hbar^2}{2m}\nabla^2\psi_{\rm im}(\boldsymbol{r},t) + V(\boldsymbol{r},t)\psi_{\rm im}(\boldsymbol{r},t) \tag{3.4}$$

$$\hbar\frac{\partial\psi_{\rm im}(\boldsymbol{r},t)}{\partial t} = \frac{\hbar^2}{2m}\nabla^2\psi_{\rm re}(\boldsymbol{r},t) - V(\boldsymbol{r},t)\psi_{\rm re}(\boldsymbol{r},t) \tag{3.5}$$

3.2.2 Discretization

In order to solve the partial differential equations numerically, it is required to transform the continuous functions into discrete functions as described below. In the following case, the spatial dimension of the wave function is fixed to one, i.e. $\psi(\boldsymbol{r},t) = \psi(x,t)$, for simplicity. Space is divided into small cells of width Δx and time is split into short steps of span Δt.

$$\psi_{\rm re}(x,t) = \psi_{\rm re}(i\Delta x, n\Delta t) \simeq R_i^n \tag{3.6}$$

$$\psi_{\rm im}(x,t) = \psi_{\rm im}(i\Delta x, n\Delta t) \simeq I_i^n \tag{3.7}$$

Next, the partial differential equations are transformed into difference equations. The Schrödinger equation contains first-order derivatives in time and second-order derivatives in space. They are calculated by using a central difference approximation as described below.

- First-order derivative in time

$$\frac{\partial\psi}{\partial t} \approx \frac{\psi(t+\frac{\Delta t}{2}) - \psi(t+\frac{\Delta t}{2})}{\Delta t} \tag{3.8}$$

- Second-order derivative in space

$$\frac{\partial^2\psi}{\partial x^2} \approx \frac{\psi(x+\Delta x) - 2\psi(x) + \psi(x-\Delta x)}{(\Delta x)^2} \tag{3.9}$$

The former approximate accuracy is $(\Delta t)^2$, and latter is $(\Delta x)^2$.

Using the above discretization, the Schrödinger equation (Eqs. (3.4) and (3.5)) is discretized and the following two equations are obtained.

$$R_i^{n+\frac{1}{2}} = R_i^{n-\frac{1}{2}} - \frac{\Delta t}{\hbar}\left[\frac{\hbar^2}{2m}\frac{I_{i+1}^n - 2I_i^n + I_{i-1}^n}{(\Delta x)^2} - V_i^n I_i^n\right] \tag{3.10}$$

$$I_i^{n+\frac{1}{2}} = I_i^{n-\frac{1}{2}} + \frac{\Delta t}{\hbar}\left[\frac{\hbar^2}{2m}\frac{R_{i+1}^n - 2R_i^n + R_{i-1}^n}{(\Delta x)^2} - V_i^n R_i^n\right] \tag{3.11}$$

3.2.3 Iteration

The calculation of Eqs. (3.10) and (3.11) at a given point i involves the points $i+1$ and $i-1$. For example, to update the real part of the wave function at the discrete point i at the instant $(n+\frac{1}{2})\Delta t$, the values of the imaginary part of the wave function at the points i, $i+1$, and $i-1$ at the instant $n\Delta t$ are required. The calculation involves the real and imaginary parts of the wave function at each node and second-order derivatives at each point of the discrete space. Therefore, in this scheme, both the real and imaginary parts of the wave function are located at the same node. This fact is different to the FDTD method applied to electromagnetic problems. The electric and magnetic field components are sampled at distinct spatial points, whereas the real and imaginary parts of wave function are calculated at the same spatial point (Fig. 3.1).

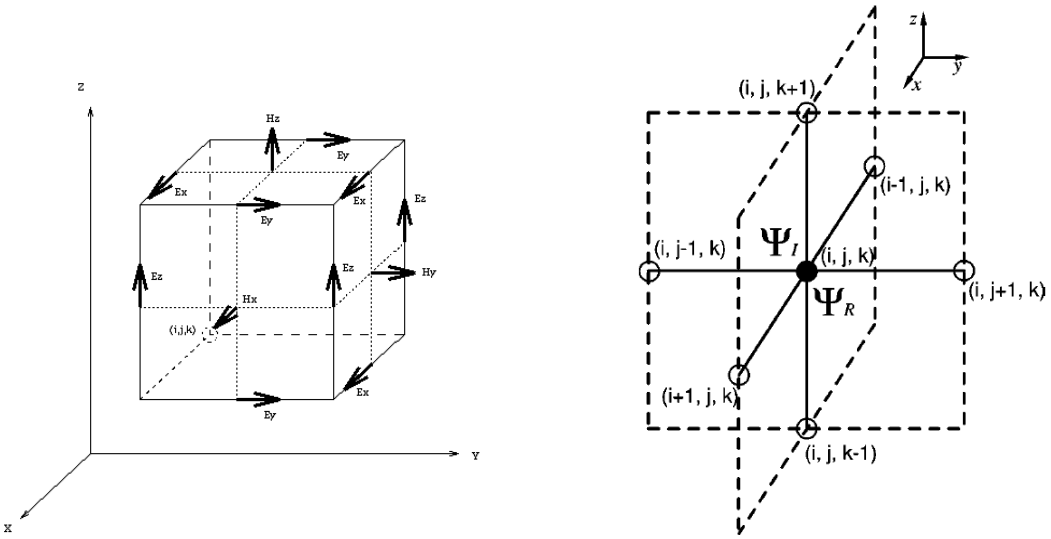

(a) Yee Cell (b) FDTD-Q Cell

Fig. 3.1: Field Components within a Cubical Grid

The time instants of the real and imaginary parts of the wave function are updated out of step with each other. The imaginary part of the wave function is out of step by a time $\frac{\Delta t}{2}$ relative to the real part. Therefore Eqs. (3.10) and (3.11) are evaluated alternately. This leapfrog manner is an analogy between the FDTD method and the FDTD-Q method.

3.2.4 Initial Value

To start this staggered algorithm, the initial values of the wave function, i.e. $\psi_{\mathrm{re}}(x,0)$ and $\psi_{\mathrm{im}}(x,\frac{\Delta t}{2})$, are necessary. An approximation is then used for estimating the initial wave function $\psi_{\mathrm{im}}(x,\frac{\Delta t}{2})$.

For example, a suitable initial state for an area without any potential is a plane wave $\psi(x,0)=\phi(x)=e^{ikx}$. The wave function is represented at the instant t by

$$\psi(x,t)=\phi(x)e^{-i\omega t}=\phi(x)e^{-i\frac{E(k)}{\hbar}t}, \tag{3.12}$$

where ω is the angular frequency and $E(k)$ is its energy. An approximation of the imaginary part of the wave function at $t=\frac{\Delta t}{2}$ may be obtained as

$$\psi_{\mathrm{im}}(x,\frac{\Delta t}{2})=-\psi_{\mathrm{re}}(x,0)\sin(\frac{E\Delta t}{2\hbar}). \tag{3.13}$$

3.2.5 Definition of Probability Density

It is not obvious in this system that the probability density is simply evaluated by

$$P=\mathrm{Re}[\psi]^2+\mathrm{Im}[\psi]^2, \tag{3.14}$$

since R and I are not defined at the same time. If one makes the choice Ref. [28],

$$P(x,t)=\psi_{\mathrm{re}}(x,n\Delta t)^2+\psi_{\mathrm{im}}(x,(n+\frac{1}{2})\Delta t)\psi_{\mathrm{im}}(x,(n-\frac{1}{2})\Delta t) \tag{3.15}$$

at integer $n=\frac{t}{\Delta t}$ and

$$P(x,t)=\psi_{\mathrm{re}}(x,(n+\frac{1}{2})\Delta t)\psi_{\mathrm{re}}(x,(n-\frac{1}{2})\Delta t)+\psi_{\mathrm{im}}(x,n\Delta t)^2 \tag{3.16}$$

at half-integer $n=\frac{t}{\Delta t}$, then it is guaranteed that the difference

$$\sum_x P(x,t+\frac{\Delta t}{2})-\sum_x P(x,t) \tag{3.17}$$

vanishes identically and therefore probability is conserved.

3.3 Stability Conditions

The time step Δt is the time increment between continuous calculations in the numerical approach described by Eqs. (3.10) and (3.11). A suitable choice of Δt is important in the FDTD-Q simulations, since the computational cost decreases as Δt increases. A larger Δt provides longer simulation time with the same number of calculation iterations. However, if Δt is too large, this makes the simulation unstable. The optimal choice of the time discretization is the largest one that keeps the algorithm stable.

In Refs. [29] and [30], the stability relationship between temporal and spatial discretizations is expressed as below inequality

$$\Delta t \leq \frac{\hbar}{\frac{\hbar^2}{m}\left[\frac{1}{(\Delta x)^2}+\frac{1}{(\Delta y)^2}+\frac{1}{(\Delta z)^2}\right]+V}. \tag{3.18}$$

The critical time step Eq. (3.18), which gives long simulation times and yet maintains the stability of the algorithm, should be used in the calculations.

3.4 Absorbing Boundary Conditions

In this section, I consider a computation area of $x = [0, N\Delta x]$, where N is a integer. From Eqs. (3.10) and (3.11), R_i^n and $I_i^{n+\frac{1}{2}}$ ($i = 1, 2, \ldots, N-1$) are calculated from R_i^{n-1}, $I_i^{n-\frac{1}{2}}$ and R_i^n. If one takes boundary conditions of $R_0^n = I_0^{n+\frac{1}{2}} = R_N^n = I_N^{n+\frac{1}{2}} = 0$ for all n, perfect reflections occur at the boundary as if an infinite potential wall existed. To avoid this reflections, it is necessary to implement absorbing boundary conditions.

3.4.1 Outline

To construct absorbing boundary conditions, the boundary should be transparent for plane waves of the form

$$\psi(x,t) = e^{-i(\omega t - kx)}. \tag{3.19}$$

This expression is only valid for scattering states. The basic idea is to build an algebraic equation for the wave vector k and the frequency ω, and then utilize the relationship between the x-t domain and the k-ω domain. In short, the correspondence of $i\frac{\partial}{\partial t} \Leftrightarrow \omega$ and $-i\frac{\partial}{\partial x} \Leftrightarrow k$ is used to construct a differential equation at the boundaries which is transparent for plane waves.

It is obvious that the boundaries are fully transparent only for plane waves and thus it is impossible to construct perfectly absorbing boundary conditions for arbitrary waves. From Eqs. (3.1), (3.2), and (3.19), the following dispersion relation for the wave vector k is obtained

$$\hbar^2 k^2 = 2m(\hbar\omega - V). \tag{3.20}$$

This equation can be solved for k and yields

$$\hbar k = \pm\sqrt{2m(\hbar\omega - V)}. \tag{3.21}$$

In this equation, the plus sign means a right-going wave and the minus sign means a left-going wave.

The absorbing boundary conditions should be constructed to satisfy the dispersion relation given by the plus-signed Eq. (3.21) at the right boundary and the minus-signed Eq. (3.21) at the left boundary. Unfortunately, Eq. (3.21) cannot be converted into an partial differential equation. Consequently, many approximation methods are proposed [31–36].

3.4.2 Padé Approximation

In Ref. [32] and others, the following Padé approximation centered at a positive constant $k = k_0$ is applied to k^2.

$$k^2 = k_0^2 \frac{-3k + k_0}{k - 3k_0} + O((k - k_0)^3) \tag{3.22}$$

Substituting the above equation into Eq. (3.20), one obtains

$$\begin{aligned} \frac{\hbar^2 k^2}{2m} \approx \frac{\hbar^2 k_0^2}{2m} \frac{-3k + k_0}{k - 3k_0} &= \hbar\omega - V \\ \frac{\hbar^2 k_0^2}{2m}(-3k + k_0) &= (k - 3k_0)(\hbar\omega - V). \end{aligned} \tag{3.23}$$

Using correspondence $i\frac{\partial}{\partial t} \Leftrightarrow \omega$ and $-i\frac{\partial}{\partial x} \Leftrightarrow k$, second absorbing boundary condition

$$\frac{\hbar^2 k_0^2}{2m}(3i\frac{\partial}{\partial x} + k_0)\psi = -(i\frac{\partial}{\partial x} + 3k_0)(i\hbar\frac{\partial}{\partial t} - V)\psi \tag{3.24}$$

is obtained. From the original Schrödinger equation,

$$(i\hbar\frac{\partial}{\partial t} - V)\psi = -\frac{\hbar^2}{2m}\frac{\partial^2\psi}{\partial x^2} \tag{3.25}$$

is guaranteed to hold. Substituting Eq. (3.25) into Eq. (3.24), one gets a new absorbing boundary condition

$$(i\frac{\partial}{\partial x} + k_0)^3\psi = 0. \tag{3.26}$$

This is a time-independent equation. Therefore, one can calculate the boundary values of the wave function from the values near the boundary at the same time.

Eq. (3.26) is separated into the real and imaginary parts in a similar way to Sec. 3.2.

$$\frac{\partial^3\psi_{\mathrm{re}}}{\partial x^3} + 3k_0\frac{\partial^2\psi_{\mathrm{im}}}{\partial x^2} - 3{k_0}^2\frac{\partial\psi_{\mathrm{re}}}{\partial x} - {k_0}^3\psi_{\mathrm{im}} = 0 \tag{3.27}$$

$$\frac{\partial^3\psi_{\mathrm{im}}}{\partial x^3} - 3k_0\frac{\partial^2\psi_{\mathrm{re}}}{\partial x^2} - 3{k_0}^2\frac{\partial\psi_{\mathrm{im}}}{\partial x} + {k_0}^3\psi_{\mathrm{re}} = 0 \tag{3.28}$$

3.4.3 Discretization

If Eqs. (3.27) and (3.28) are discretized, we will obtain difference equations. However, at the boundary, the central difference method is impractical, since the values in outer domain are not defined. We will therefore employ the forward and backward difference methods in this case. Specifically, the forward difference method is applied at the left boundary ($x = 0$) and the backward difference method is applied at the right boundary ($x = N\Delta x$).

Left Boundary

The derivatives are approximated in the following forward difference method as follows:

- The 1st-order derivative

$$\frac{\partial \psi}{\partial x} \approx \frac{\psi(\Delta x) - \psi(0)}{\Delta x} \tag{3.29}$$

- The 2nd-order derivative

$$\frac{\partial^2 \psi}{\partial x^2} \approx \frac{\psi(2\Delta x) - 2\psi(\Delta x) + \psi(0)}{(\Delta x)^2} \tag{3.30}$$

- The 3rd-order derivative

$$\frac{\partial^3 \psi}{\partial x^3} \approx \frac{\psi(3\Delta x) - 3\psi(2\Delta x) + 3\psi(\Delta x) - \psi(0)}{(\Delta x)^3} \tag{3.31}$$

Eqs. (3.27) and (3.28) are modified into the following difference equations

$$\frac{R_3 - 3R_2 + 3R_1 - R_0}{(\Delta x)^3} + 3k_0 \frac{I_2 - 2I_1 + I_0}{(\Delta x)^2} - 3{k_0}^2 \frac{R_1 - R_0}{\Delta x} - {k_0}^3 I_0 = 0 \tag{3.32}$$

$$\frac{I_3 - 3I_2 + 3I_1 - I_0}{(\Delta x)^3} - 3k_0 \frac{R_2 - 2R_1 + R_0}{(\Delta x)^2} - 3{k_0}^2 \frac{I_1 - I_0}{\Delta x} + {k_0}^3 R_0 = 0. \tag{3.33}$$

They are solved for R_0 and I_0 which then yields

$$\begin{aligned} R_0 &= \frac{3}{a^2+1} R_1 + \frac{3(a^2-1)}{(a^2+1)^2} R_2 - \frac{3a^2-1}{(a^2+1)^3} R_3 \\ &\quad + \frac{3a}{a^2+1} I_1 - \frac{6a}{(a^2+1)^2} I_2 - \frac{a(a^2-3)}{(a^2+1)^3} I_3 \end{aligned} \tag{3.34}$$

$$\begin{aligned} I_0 &= -\frac{3a}{a^2+1} R_1 + \frac{6a}{(a^2+1)^2} R_2 + \frac{a(a^2-3)}{(a^2+1)^3} R_3 \\ &\quad + \frac{3}{a^2+1} I_1 + \frac{3(a^2-1)}{(a^2+1)^2} I_2 - \frac{3a^2-1}{(a^2+1)^3} I_3 \end{aligned} \tag{3.35}$$

with $a = k_0 \Delta x$.

Right Boundary

The derivatives are approximated in the following backward difference method as follows:

- The 1st-order derivative

$$\frac{\partial \psi}{\partial x} \approx \frac{\psi(N\Delta x) - \psi((N-1)\Delta x)}{\Delta x} \tag{3.36}$$

- The 2nd-order derivative

$$\frac{\partial^2 \psi}{\partial x^2} \approx \frac{\psi(N\Delta x) - 2\psi((N-1)\Delta x) + \psi((N-2)\Delta x)}{(\Delta x)^2} \tag{3.37}$$

- The 3rd-order derivative

$$\frac{\partial^3 \psi}{\partial x^3} \approx \frac{\psi(N\Delta x) - 3\psi((N-1)\Delta x) + 3\psi((N-2)\Delta x) - \psi((N-3)\Delta x)}{(\Delta x)^3} \tag{3.38}$$

Eqs. (3.27) and (3.28) are modified into the following difference equations:

$$\frac{R_N - 3R_{N-1} + 3R_{N-2} - R_{N-3}}{(\Delta x)^3} + 3k_0\frac{I_N - 2I_{N-1} + I_{N-2}}{(\Delta x)^2} - 3{k_0}^2\frac{R_N - R_{N-1}}{\Delta x} - {k_0}^3 I_N = 0 \tag{3.39}$$

$$\frac{I_N - 3I_{N-1} + 3I_{N-2} - I_{N-3}}{(\Delta x)^3} - 3k_0\frac{R_N - 2R_{N-1} + R_{N-2}}{(\Delta x)^2} - 3{k_0}^2\frac{I_N - I_{N-1}}{\Delta x} + {k_0}^3 R_N = 0. \tag{3.40}$$

They are solved for R_N and I_N which then yields

$$\begin{aligned} R_N &= \frac{3}{a^2+1}R_{N-1} + \frac{3(a^2-1)}{(a^2+1)^2}R_{N-2} - \frac{3a^2-1}{(a^2+1)^3}R_{N-3} \\ &\quad - \frac{3a}{a^2+1}I_{N-1} + \frac{6a}{(a^2+1)^2}I_{N-2} + \frac{a(a^2-3)}{(a^2+1)^3}I_{N-3} \end{aligned} \tag{3.41}$$

$$\begin{aligned} I_N &= \frac{3a}{a^2+1}R_{N-1} - \frac{6a}{(a^2+1)^2}R_{N-2} - \frac{a(a^2-3)}{(a^2+1)^3}R_{N-3} \\ &\quad + \frac{3}{a^2+1}I_{N-1} + \frac{3(a^2-1)}{(a^2+1)^2}I_{N-2} - \frac{3a^2-1}{(a^2+1)^3}I_{N-3} \end{aligned} \tag{3.42}$$

with $a = k_0\Delta x$.

3.4.4 Energy-weighted Wave-number Parameter

The parameter k_0 plays the role of the expansion point in the Padé approximation. In the above absorbing boundary conditions, it needs to be pre-estimated. Therefore, one of the most important issues is how to select a suitable k_0 such that it minimize the reflection of the wave at the boundary. In the following, for convenience, the discussion is focused on the right boundary ($x = N\Delta x$).

It is most constructive to estimate the parameter in the frequency domain. The wave function at time t is able to be expressed in terms of a Fourier series. In Ref. [35], a general strategy is given to estimate the wave-number parameter k_0, which is a function of time t. The strategy is to use a discrete Fourier series expansion of the physical variable in space

$$\hat{\psi}(\chi, t) = \sum_{j=0}^{N} \psi(x_j, t) e^{-i\chi x_j \frac{2\pi}{L}} \qquad (\text{ for } \quad \chi = -\frac{N}{2}, -\frac{N}{2}+1, \ldots, \frac{N}{2}\ ) \tag{3.43}$$

with $x_0 = 0$, $x_N = L$ and N even. If a certain Fourier mode is dominant, one can choose the parameter $k_0 = \frac{2\pi}{L}\chi_0$ such that

$$|\hat{\psi}(\chi_0, t)| = \max_{0 \le \chi \le \frac{N}{2}} \{\ |\hat{\psi}(\chi, t)|\ \}. \tag{3.44}$$

Eq. (3.44) is not the best choice in many practical cases. When two Fourier modes are both dominant, it is obvious that the best choice of the parameter to minimize the reflection is the medial value of the

two different wave numbers. Consequently, an improvement is to use a weighting strategy [34]. The approach is to weight the energy as follows,

$$k_0 = \frac{2\pi}{L} \sum_{\chi=0}^{\frac{N}{2}} \{|\hat{\psi}(\chi,t)|^p \chi)\} \Big/ \sum_{\chi=0}^{\frac{N}{2}} |\hat{\psi}(\chi,t)|^p, \tag{3.45}$$

with p a positive real number. When $p \to +\infty$, Eq. (3.45) converges to Eq. (3.44). In Ref. [34], the authors suggest that $p = 4$ is a good choice based on numerical experiments.

3.5 The FDTD-Q Algorithm (Imaginary Time)

The Schrödinger equation provides the general description of microscopic phenomena. However the Schrödinger equation is analytically solvable only in a few highly idealized cases and thus, for realistic systems, one needs to resort to numerical solutions. Recently the Diffusion Monte Carlo method was introduced for these analytically unsolvable systems [37–39]. This method is suitable for obtaining the ground state of many complicated quantum systems. However the method that works best for simple systems, such as systems without local potential minima, is the imaginary time evolution method [40, 41], which is the basic concept of the Diffusion Monte Carlo method and is described below.

3.5.1 Imaginary-time Evolution

The solution of the time-dependent Schrödinger equation can be written in general as a linear superposition of stationary states with the time dependence given by the phase factor $\exp(-iE_n t/\hbar)$, where E_n is the n-th energy level of the quantum system. The energy can be chosen such that all energies are positive.

Now, if we consider in imaginary time, that is to say, replacing the time t by $-i\tau$, the solution of the Schrödinger equation is given by a sum of transients of the form $\exp(-E_n\tau/\hbar)$. As the quantum system evolves in imaginary time, the longest surviving transient corresponds to the ground state (the state with the lowest possible energy E_0) of the system. Consequently, evolved for adequately long in imaginary time, one can obtain both the ground state energy E_0 and the ground state wave function ϕ_0 of the quantum system. Moreover, this method is not sensitive to the initial state prepared.

3.5.2 Numerical Scheme

The numerical scheme for the imaginary-time Schrödinger equation is basically similar to the scheme for the real-time Schrödinger equation described in Sec. 3.2. The Schrödinger equation in imaginary time is as follows,

$$-\hbar \frac{\partial \psi(\boldsymbol{r},\tau)}{\partial \tau} = \hat{H}\psi(\boldsymbol{r},\tau), \tag{3.46}$$

where the Hamiltonian has the form

$$\hat{H} = -\frac{\hbar^2}{2m}\nabla^2 + V(\boldsymbol{r}). \tag{3.47}$$

Separating the wave function into real and imaginary parts, one obtains the following two equations:

$$\hbar\frac{\partial\psi_{\rm re}(\boldsymbol{r},\tau)}{\partial\tau} = \frac{\hbar^2}{2m}\nabla^2\psi_{\rm re}(\boldsymbol{r},\tau) - V(\boldsymbol{r})\psi_{\rm re}(\boldsymbol{r},\tau) \tag{3.48}$$

$$\hbar\frac{\partial\psi_{\rm im}(\boldsymbol{r},\tau)}{\partial\tau} = \frac{\hbar^2}{2m}\nabla^2\psi_{\rm im}(\boldsymbol{r},\tau) - V(\boldsymbol{r})\psi_{\rm im}(\boldsymbol{r},\tau). \tag{3.49}$$

Then, discretizing the wave function, one obtains the following two equations,

$$R_i^{n+1} = R_i^n + \frac{\Delta t}{\hbar}\left[\frac{\hbar^2}{2m}\frac{R_{i+1}^n - 2R_i^n + R_{i-1}^n}{(\Delta x)^2} - V_i R_i^n\right] \tag{3.50}$$

$$I_i^{n+1} = I_i^n + \frac{\Delta t}{\hbar}\left[\frac{\hbar^2}{2m}\frac{I_{i+1}^n - 2I_i^n + I_{i-1}^n}{(\Delta x)^2} - V_i I_i^n\right], \tag{3.51}$$

in the one-dimensional case.

Chapter 4

Implementation of FDTD-Q Simulations for a Two-particle System

4.1 Overview

4.1.1 Two-particle Two-site System

To analyse the nature of a Mott insulator phase, particularly to find the state of each particle, it is necessary to calculate the wave function of the system. Let us consider two electrons trapped in a plane, e.g. a two-dimensional electron gas (2DEG) in a GaAs/AlGaAs heterojunction. In this chapter, I will consider a two-electron system where the two electrons are trapped in a two-site geometry (see Fig. 4.1). The electrons are confined within the area:

$$D = \{\, (x,z) \mid 0 < x < L_x,\ 0 < z < L_z \,\} \tag{4.1}$$

in the x-z plane. The external confining potential V_{ext} is described as

$$\begin{cases} V_{\text{ext}} = 0 & (\ (x,z) \in D\ ) \\ V_{\text{ext}} = \infty & (\ \text{else}\ ) \end{cases} . \tag{4.2}$$

The lattice potential V_{lat} is modulated only in x-direction and written

$$V_{\text{lat}}(x,t) = V(t)\cos\left(\frac{4\pi x}{L_x}\right), \tag{4.3}$$

where $V(t) \geq 0$ is the time-transient lattice potential depth.

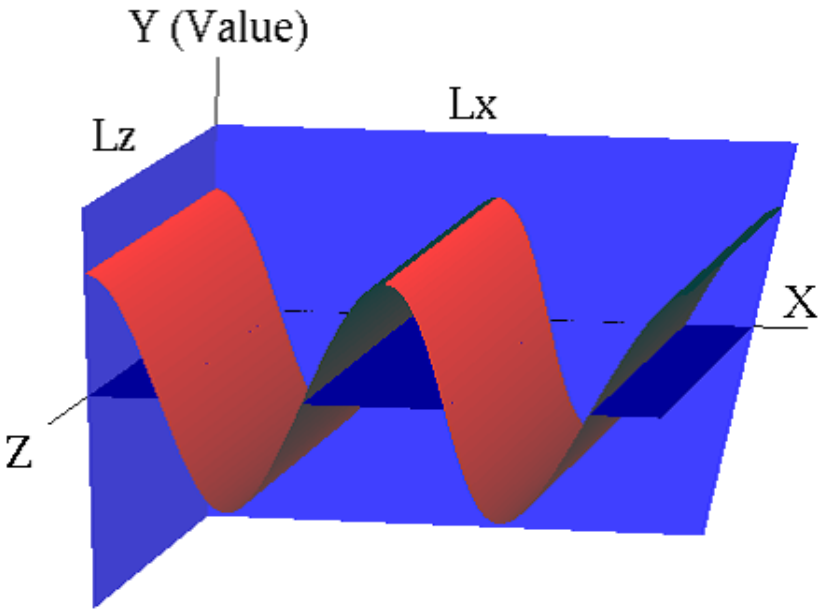

Fig. 4.1: Lattice Potential in the Two-Site Model

4.1.2 Conceptual Expression of the Ground State in the Two-site Model

In this two-site geometry, the ground state of a single electron is simply and conceptually expressed by two basic states $|L\rangle$ and $|R\rangle$, or their superposition state. The $|L\rangle$ state corresponds to a state where

the electron is mostly found on the left site ($0 \leq x \leq \frac{L_x}{2}$). On the other hand, the $|R\rangle$ state corresponds to a state where the electron is mostly found on the right site ($\frac{L_x}{2} \leq x \leq L_x$). The single-electron ground state of this model is then

$$|\Phi\rangle = \frac{1}{\sqrt{2}}(|L\rangle + |R\rangle). \tag{4.4}$$

The ground state of the two-electron system without any interaction is then written

$$\begin{aligned} |\Psi\rangle_{U=0} &= \frac{1}{\sqrt{2}}(|L\rangle + |R\rangle)_1 \otimes \frac{1}{\sqrt{2}}(|L\rangle + |R\rangle)_2 \\ &= \frac{1}{2}(|LL\rangle + |LR\rangle + |RL\rangle + |RR\rangle), \end{aligned} \tag{4.5}$$

where

$$|LL\rangle = |L\rangle_1 \otimes |L\rangle_2 \tag{4.6}$$
$$|LR\rangle = |L\rangle_1 \otimes |R\rangle_2 \tag{4.7}$$
$$|RL\rangle = |R\rangle_1 \otimes |L\rangle_2 \tag{4.8}$$
$$|RR\rangle = |R\rangle_1 \otimes |R\rangle_2. \tag{4.9}$$

Using this expression, we may guess that the ground state of the system with interactions might be given by

$$|\Psi\rangle_{U\neq 0} = \frac{1}{\sqrt{2}}(|LR\rangle + |RL\rangle) \tag{4.10}$$

since $|LL\rangle$ and $|RR\rangle$ states contain the higher interaction energy.

4.1.3 Time Evolution

The lattice potential V_{lat} corresponding to the tunneling (hopping) term may only be a tunable parameter in nature because it is applied externally. However, exploiting the calculation techniques, the interaction term is also controllable and can even be set to zero.

While controlling these two parameters, we simulate the time evolution of the system. Beginning in the ground state of the system, the system remains in the ground state as long as the condition of adiabatic evolution is observed. We may thereby calculate the ground state for all interaction energies.

4.1.4 Phase Observation

A transient phase of the system is observed in the form of interference patterns after a free expansion. This was also seen in the experiment of Greiner et al [17]. After the two electrons are released from both the external confining potential and the lattice potential, they freely propagate through the x-z plane while interfering with each other.

In the experiment of Greiner et al., the phase is perfectly coherent over the entire lattice in a Bose-Einstein condensate state and therefore only the first-order interference maximum is visible (Fig. 2.6a). In a superfluid state, all atoms are localized throughout the entire lattice with equal relative phases between different lattice sites and, thus, higher-order interference maxima are visible (Fig. 2.6b-d). On the other hand, in a Mott insulator state, since each of atoms are localized on an individual site, no interference pattern is visible (Fig. 2.6g, h).

As described above, higher-order interference maxima should be visible in a metal (conducting) phase of this system, while only a blurry and broadened interference pattern should be observed in a Mott insulator (insulating) phase in this calculation.

4.2 Implementation

4.2.1 Hamiltonian

In a N-body system where each particle has the mass m_i, the Hamiltonian of the system is described in the following form:

$$\hat{H}_{N-\mathrm{body}} = \sum_{i=1}^{N} \left(-\frac{\hbar^2}{2m_i} {\nabla_i}^2 + V_i(\boldsymbol{r_i}, t) \right) + \sum_{i \neq k} V_{i,k}(\boldsymbol{r_i}, \boldsymbol{r_k}). \tag{4.11}$$

V_i is the single-body potential for the i-th particle. It depends on the position $\boldsymbol{r_i}$ and also time t. $V_{i,k}$ is the potential of interaction between the i-th and k-th particles. It depends on the both positions $\boldsymbol{r_i}$ and $\boldsymbol{r_k}$. Usually $V_{i,k}$ is a function of the relative position $|\boldsymbol{r_i} - \boldsymbol{r_k}|$. The N-body Schrödinger equation is then written

$$\hat{H}_{N-\mathrm{body}} \Psi(\boldsymbol{r_1}, \boldsymbol{r_2}, \ldots, \boldsymbol{r_N}, t) = i\hbar \frac{\partial}{\partial t} \Psi(\boldsymbol{r_1}, \boldsymbol{r_2}, \ldots, \boldsymbol{r_N}, t). \tag{4.12}$$

Let us consider the situation of two particles confined in the x-z plane, where an external potential is modulated only in x-direction. Eq. (4.11) is then rewritten

$$\begin{aligned} \hat{H}_{2-\mathrm{body}} \quad = \quad & -\frac{\hbar^2}{2m_1}\left(\frac{\partial^2}{\partial x_1^2} + \frac{\partial^2}{\partial z_1^2} \right) - \frac{\hbar^2}{2m_2}\left(\frac{\partial^2}{\partial x_2^2} + \frac{\partial^2}{\partial z_2^2} \right) \\ & + V_1(x_1, t) + V_2(x_2, t) + V_{1,2}(x_1, z_1, x_2, z_2), \end{aligned} \tag{4.13}$$

where $V_{1,2}$ is the potential of the Coulomb interaction between two particles and, thus, has the following form:

$$V_{1,2}(x_1, z_1, x_2, z_2) = \frac{e^2}{4\pi\varepsilon_{\mathrm{r}}\varepsilon_0} \frac{1}{\sqrt{(x_1 - x_2)^2 + (z_1 - z_2)^2}}, \tag{4.14}$$

where we have the elementary charge e, the permittivity of free space ε_0, and the relative permittivity ε_{r}. See Appendix A for numerical values used. In addition, Eq. (4.12) is rewritten

$$\hat{H}_{2-\mathrm{body}} \Psi(x_1, z_1, x_2, z_2, t) = i\hbar \frac{\partial}{\partial t} \Psi(x_1, z_1, x_2, z_2, t). \tag{4.15}$$

In the following, I assume that the two electrons have the same mass ($m_1 = m_2 = m_{\rm e}^*$) and anti-parallel spins, that is to say, one has an up-spin ($\uparrow$) and the other has a down-spin ($\downarrow$), and also assume that the spin part of the wave function of the system is antisymmetrized. In this way we interpret the ground state of the system for two electrons, which are fermions. (Note that one can also consider a boson version if assumes two spin less particles.)

4.2.2 Probability Density

The probability density that the first-indexed electron is found at (x_1, z_1) and the second-indexed electron is found at (x_2, z_2) at a same time t is given by

$$P(x_1, z_1, x_2, z_2, t) = |\Psi(x_1, z_1, x_2, z_2, t)|^2. \tag{4.16}$$

In this system, since the two lattice sites are aligned along the x-axis, the probability density distribution of z-direction is not physically important. Because we are interested in which site the particle exists, there is a need for calculate the following probability densities:

$$P(x_1, x_2, t) = \int\int P(x_1, z_1, x_2, z_2, t) dz_1 dz_2 \tag{4.17}$$

$$P(x_1, t) = \int P(x_1, x_2, t) dx_2 \tag{4.18}$$

$$P(x_2, t) = \int P(x_1, x_2, t) dx_1 \tag{4.19}$$

$$\tag{4.20}$$

4.2.3 Discretization (Real Time)

To calculate the wave function using the FDTD-Q algorithm described in Sec. 3.2, the wave function has to be separated into its real and imaginary parts and discretized. We must therefore transform the two-body Schrödinger equation (Eq. (4.15)) into difference equations. Let us here define the second-order differences as the following equations:

$$DiffXR^n_{i_1,j_1,i_2,j_2} = \frac{R^n_{i_1+1,j_1,i_2,j_2} + R^n_{i_1-1,j_1,i_2,j_2} + R^n_{i_1,j_1,i_2+1,j_2} + R^n_{i_1,j_1,i_2-1,j_2} - 4R^n_{i_1,j_1,i_2,j_2}}{(\Delta x)^2} \tag{4.21}$$

$$DiffZR^n_{i_1,j_1,i_2,j_2} = \frac{R^n_{i_1,j_1+1,i_2,j_2} + R^n_{i_1,j_1-1,i_2,j_2} + R^n_{i_1,j_1,i_2,j_2+1} + R^n_{i_1,j_1,i_2,j_2-1} - 4R^n_{i_1,j_1,i_2,j_2}}{(\Delta z)^2} \tag{4.22}$$

$$DiffXI^n_{i_1,j_1,i_2,j_2} = \frac{I^n_{i_1+1,j_1,i_2,j_2} + I^n_{i_1-1,j_1,i_2,j_2} + I^n_{i_1,j_1,i_2+1,j_2} + I^n_{i_1,j_1,i_2-1,j_2} - 4I^n_{i_1,j_1,i_2,j_2}}{(\Delta x)^2} \tag{4.23}$$

$$DiffZI^n_{i_1,j_1,i_2,j_2} = \frac{I^n_{i_1,j_1+1,i_2,j_2} + I^n_{i_1,j_1-1,i_2,j_2} + I^n_{i_1,j_1,i_2,j_2+1} + I^n_{i_1,j_1,i_2,j_2-1} - 4I^n_{i_1,j_1,i_2,j_2}}{(\Delta z)^2}, \tag{4.24}$$

with cell size $\Delta x = \frac{L_x}{N_x}$, $\Delta z = \frac{L_z}{N_z}$ and position indexes i_1, i_2, j_1, j_2. Parameters $i_1, i_2 \in \{i | i = 0, 1, \ldots, N_x\}$ and $j_1, j_2 \in \{j | j = 0, 1, \ldots, N_z\}$ correspond to x_1, x_2, z_1, and z_2 respectively, that is, for example, $x_1 = i_1 \Delta x$. Using the above definitions, the Schrödinger equation is transformed into the following two difference equations:

$$R^{n+\frac{1}{2}}_{i_1,j_1,i_2,j_2} = R^{n-\frac{1}{2}}_{i_1,j_1,i_2,j_2} - \frac{\hbar \Delta t}{2m_{\rm e}^*} \left\{ DiffXI^n_{i_1,j_1,i_2,j_2} + DiffZI^n_{i_1,j_1,i_2,j_2} \right\}$$

$$+\frac{\Delta t}{\hbar}\left\{V_{i_1}^n + V_{i_2}^n + \frac{e^2}{4\pi\varepsilon_{\mathrm{r}}\varepsilon_0}\frac{1}{\sqrt{(i_1-i_2)^2(\Delta x)^2+(j_1-j_2)^2(\Delta z)^2}}\right\}I_{i_1,j_1,i_2,j_2}^n \tag{4.25}$$

$$I_{i_1,j_1,i_2,j_2}^{n+\frac{1}{2}} = I_{i_1,j_1,i_2,j_2}^{n-\frac{1}{2}} + \frac{\hbar\Delta t}{2m_{\mathrm{e}}^*}\left\{DiffXR_{i_1,j_1,i_2,j_2}^n + DiffZR_{i_1,j_1,i_2,j_2}^n\right\}$$
$$-\frac{\Delta t}{\hbar}\left\{V_{i_1}^n + V_{i_2}^n + \frac{e^2}{4\pi\varepsilon_{\mathrm{r}}\varepsilon_0}\frac{1}{\sqrt{(i_1-i_2)^2(\Delta x)^2+(j_1-j_2)^2(\Delta z)^2}}\right\}R_{i_1,j_1,i_2,j_2}^n \tag{4.26}$$

When the indexes satisfy to $(i_1, j_1) = (i_2, j_2)$, the Coulomb potential diverges. Therefore the values of the wave function are fixed to 0 at those cells.

$$R_{i,j,i,j}^n = I_{i,j,i,j}^n = 0, \qquad \forall i, j, n \tag{4.27}$$

In this calculation, I employed the parameters described in Tab. 4.1:

Tab. 4.1: Parameters for the Simulation of a Two-particle System

Name	Symbol	Value	Unit
Width	L_x	2.0×10^{-7}	m
Depth	L_z	1.0×10^{-7}	m
Cell Number for x-direction	N_x	20	–
Cell Number for z-direction	N_z	8	–
Time Step	Δt	1.0×10^{-15}	s

4.2.4 Discretization (Imaginary Time)

Using Eqs. (4.21) - (4.24), the imaginary time evolution is formulated in a similar way.

$$R_{i_1,j_1,i_2,j_2}^{n+\frac{1}{2}} = R_{i_1,j_1,i_2,j_2}^{n-\frac{1}{2}} + \frac{\hbar\Delta t}{2m_{\mathrm{e}}^*}\left\{DiffXR_{i_1,j_1,i_2,j_2}^n + DiffZR_{i_1,j_1,i_2,j_2}^n\right\}$$
$$-\frac{\Delta t}{\hbar}\left\{V_{i_1}^n + V_{i_2}^n + \frac{e^2}{4\pi\varepsilon_{\mathrm{r}}\varepsilon_0}\frac{1}{\sqrt{(i_1-i_2)^2(\Delta x)^2+(j_1-j_2)^2(\Delta z)^2}}\right\}R_{i_1,j_1,i_2,j_2}^n \tag{4.28}$$

$$I_{i_1,j_1,i_2,j_2}^{n+\frac{1}{2}} = I_{i_1,j_1,i_2,j_2}^{n-\frac{1}{2}} + \frac{\hbar\Delta t}{2m_{\mathrm{e}}^*}\left\{DiffXI_{i_1,j_1,i_2,j_2}^n + DiffZI_{i_1,j_1,i_2,j_2}^n\right\}$$
$$-\frac{\Delta t}{\hbar}\left\{V_{i_1}^n + V_{i_2}^n + \frac{e^2}{4\pi\varepsilon_{\mathrm{r}}\varepsilon_0}\frac{1}{\sqrt{(i_1-i_2)^2(\Delta x)^2+(j_1-j_2)^2(\Delta z)^2}}\right\}I_{i_1,j_1,i_2,j_2}^n \tag{4.29}$$

4.2.5 Absorbing Boundary Conditions

If two electrons are released from an external confining potential and a lattice potential, they freely expand in the plane. However computational resources restrict vast-area calculations. Consequently there is a need for implementing absorbing boundary conditions to calculate the propagation in a small area and to save resources.

The absorbing boundary condition formula represented by Eq. (3.26) can be applied to all coordinates. The implementation described in Sec. 3.4 can be used to modify the indices of Eqs. (3.34), (3.35), (3.41), and (3.42).

4.3 Experimental Procedure

4.3.1 Initial State

Without any lattice potential and any interaction, i.e., $V_1 = V_2 = V_{1,2} = 0$, the single-electron wave function of the ground state is given by

$$\phi_i(x_i, z_i) = \frac{2}{\sqrt{L_x L_z}} \sin\left(\frac{\pi x_i}{L_x}\right) \sin\left(\frac{\pi z_i}{L_z}\right), \tag{4.30}$$

and the ground-state energy of a single electron is also given by

$$E_{\mathrm{GS}} = \frac{\pi^2 \hbar^2}{2m_{\mathrm{e}}^*}\left(\frac{1}{{L_x}^2} + \frac{1}{{L_z}^2}\right) \tag{4.31}$$

The wave function of the system is then written

$$\begin{aligned} \Phi(x_1, z_1, x_2, z_2) &= \phi_1(x_1, z_1)\phi_2(x_2, z_2) \\ &= \frac{4}{L_x L_z} \sin\left(\frac{\pi x_1}{L_x}\right) \sin\left(\frac{\pi z_1}{L_z}\right) \sin\left(\frac{\pi x_2}{L_x}\right) \sin\left(\frac{\pi z_2}{L_z}\right). \end{aligned} \tag{4.32}$$

Following the description in Sec. 3.2, one obtains the following discretized initial values:

$$R^0_{i_1,j_1,i_2,j_2} = \frac{4}{L_x L_z} \sin\left(\frac{\pi i_1}{N_x}\right) \sin\left(\frac{\pi j_1}{N_z}\right) \sin\left(\frac{\pi i_2}{N_x}\right) \sin\left(\frac{\pi j_2}{N_z}\right) \tag{4.33}$$

$$I^{\frac{1}{2}}_{i_1,j_1,i_2,j_2} = -R^0_{i_1,j_1,i_2,j_2} \sin\left(\frac{E_{\mathrm{GS}}\Delta t}{\hbar}\right). \tag{4.34}$$

4.3.2 Increasing the Lattice Potential

As the lattice potential is gradually increased, without any interaction, both two electrons start to localize on each lattice site. For large lattice potentials, each electron will be in a superposition state of a left on-site state and a right on-site state. In this state, the electron can hop from the left site to the right site, and vice versa. The wave function of the system has the form of Eq. (4.5).

In this simulation, the lattice potential was increased with a step $\Delta V = 1.0 \times 10^{-26}$[J] during half a step ($\frac{\Delta t}{2}$). The increment continued from $t = 0$ to $t = 10^4 \Delta t$.

4.3.3 Increasing Both the Interaction Term and the Lattice Potential

After switching on the interaction term at $t = 0$, to calculate the ground state of an interacting system, an imaginary time evolution is performed for some time until the ground state is obtained. As the lattice potential is gradually increased in real time, electrons become localized on each site.

In this simulation, the imaginary time evolution was iterated for 10^4 steps. After this, the lattice potential was increased with a step $\Delta V = 1.0 \times 10^{-26}$[J] for every half a step ($\frac{\Delta t}{2}$). This was continued from $t = 10^4 \Delta t$ to $t = 2 \times 10^4 \Delta t$.

4.3.4 Free Expansion

Released from both the external confining potential and the lattice potential after the time evolution, the electrons scatter freely and interfere with each other. In this scattering process, only the propagation along the x-axis was calculated, for the electrons do not interfere as much along the z-direction due to the x-directional site alignment. Furthermore, the interaction term is set to zero again since it no longer affects the correlation between the two electrons after localization.

4.4 Results and Speculations

In this section, I will show two types of figures. The figures with red and blue line graphs show the probability density distribution as a function of x. The red line indicates the first indexed electron and the blue line indicates the second indexed electron. The figures with black envelopes and colored inners show the conditional probability density distribution as a function of x on the condition that the opposite electron is found at the vertically lined position. The inner color indicates the relative phase (see Appendix B). In the both types of figure, the green line indicates the shape of the lattice potential.

4.4.1 Initial State

The initial state is given by Eq. (4.32). This is plotted in Figs. 4.2 and 4.3. The wave function of the initial state without any interaction and any lattice potential is spread over the whole area with perfect phase coherence.

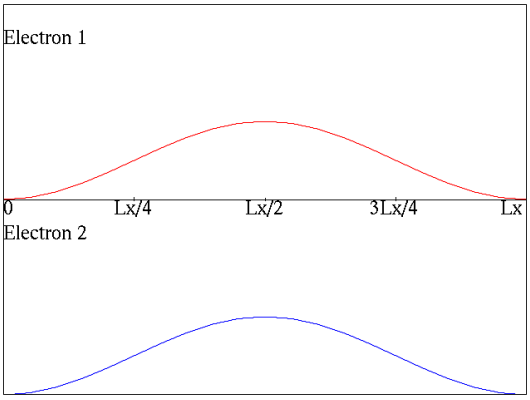

Fig. 4.2: Probability Density Distribution of the Initial State

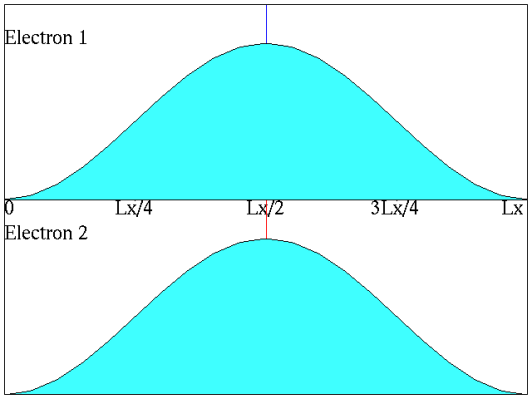

Fig. 4.3: Conditional Probability Density Distribution of the Initial State

After being released from the external confining potential, the two electrons freely expand and interfere with each other. In Figs. 4.4 and 4.5, only the first-order maximum is visible at the center.

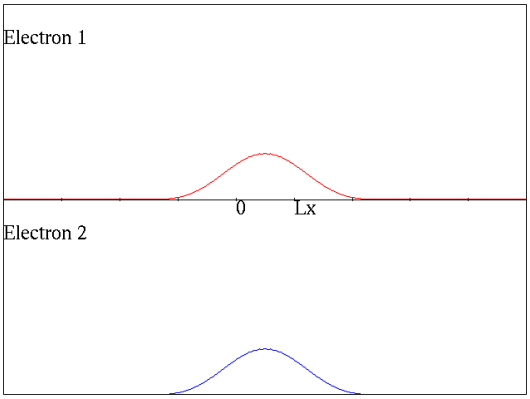

Fig. 4.4: Interference Pattern of the Initial State

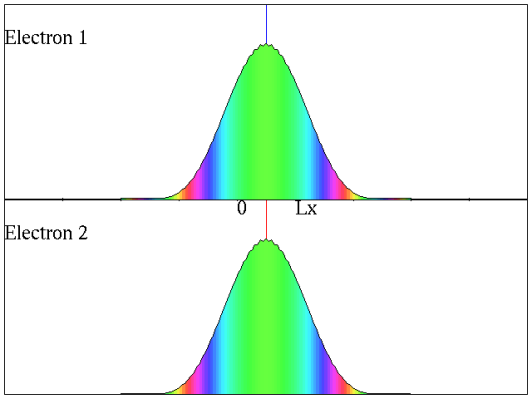

Fig. 4.5: Conditional Interference Pattern of the Initial State

4.4.2 Regime with Hopping

After the lattice potential is increased, the electrons localize on both sites with equal phase (see Figs. 4.6 and 4.7). In Fig. 4.7, we see that the left and right sides of the single-electron wave function are in phase.

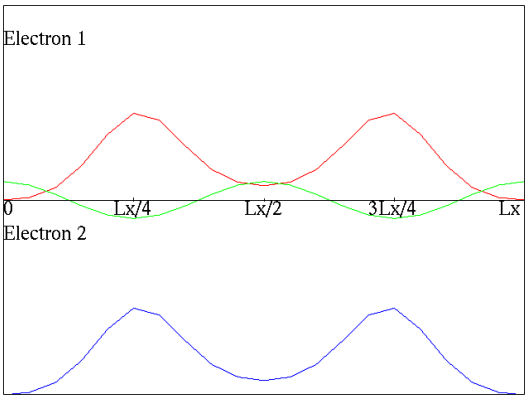

Fig. 4.6: Probability Density Distribution of a Regime with Hopping

After being released from the external confining potential and the lattice potential, the two electrons freely expand and interfere with each other. In Figs. 4.8 and 4.9, we see higher-order maxima. Furthermore, in Fig. 4.9, we see that the interference maxima are always visible wherever the opposite electron is found. Consequently, as the sum of these phenomena, the probability density distribution (Fig. 4.8) also shows the interference maxima.

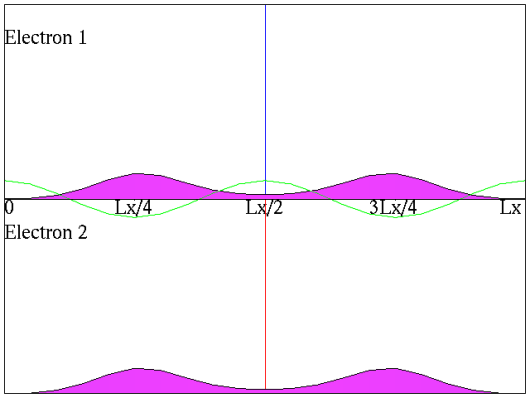

(a) When one is found at the center, the other can be found on both sites.

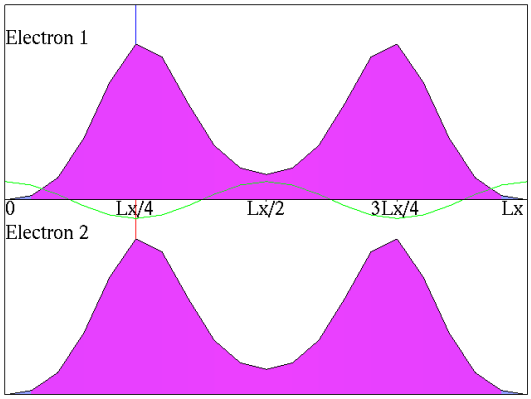

(b) When one is found on the left site, the other can be found on both sites.

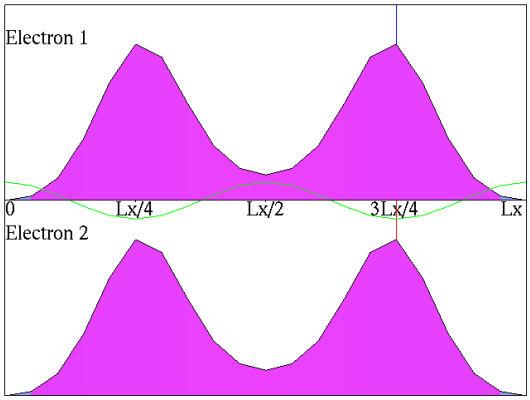

(c) When one is found on the right site, the other can be found on both sites.

Fig. 4.7: Conditional Probability Density Distribution of a Regime with Hopping

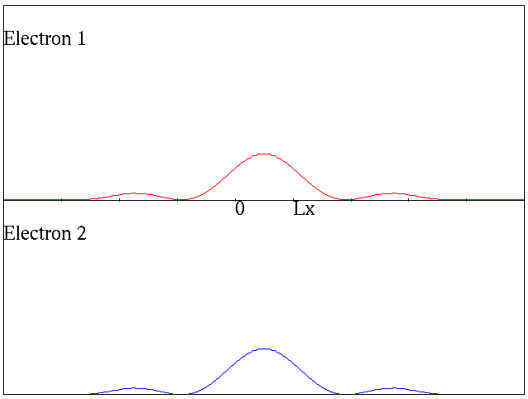

Fig. 4.8: Interference Pattern of a Regime with Hopping

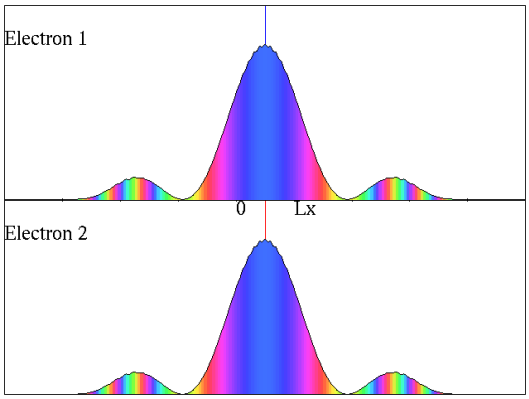

(a) First-order Maximum

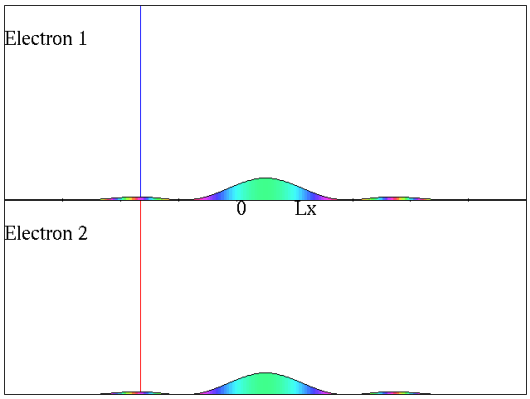

(b) Left-side Peak

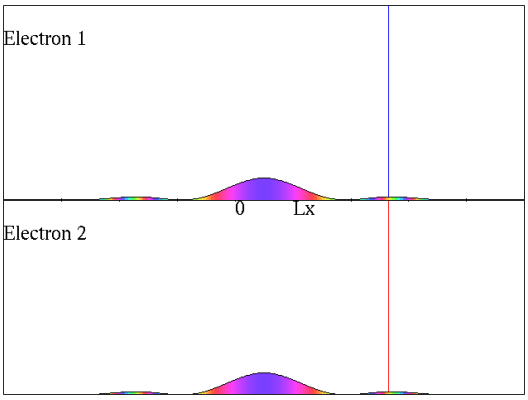

(c) Right-side Peak

Fig. 4.9: Conditional Interference Pattern of a Regime with Hopping

This state can be written

$$|\Psi\rangle = \frac{1}{2}(|L\rangle + |R\rangle)_1 \otimes (|L\rangle + |R\rangle)_2. \tag{4.35}$$

Both electrons can hop from one site to the other site respectively. This phase consists of the quantum superposition state of each particle and, consequently, can be thought to be a metal phase, or a superfluid phase if considering the experiment of Greiner et al.

4.4.3 Regime with Hopping and Interaction

After the imaginary time evolution and the increase of the lattice potential, the electrons begin localizing on an individual site (see Figs. 4.10 and 4.11). This state has a correlation between electron positions. That is to say, if one electron is found on one site, the other electron is found on the opposite site.

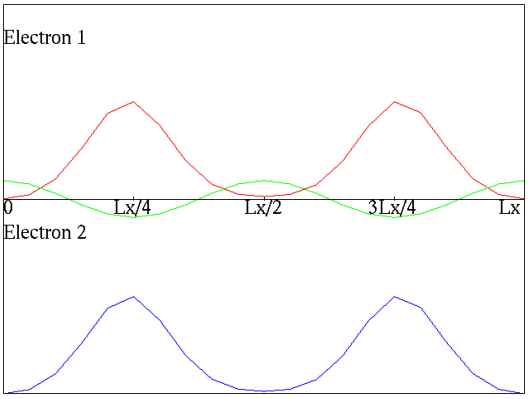

Fig. 4.10: Probability Density Distribution of a Regime with Hopping and Interaction

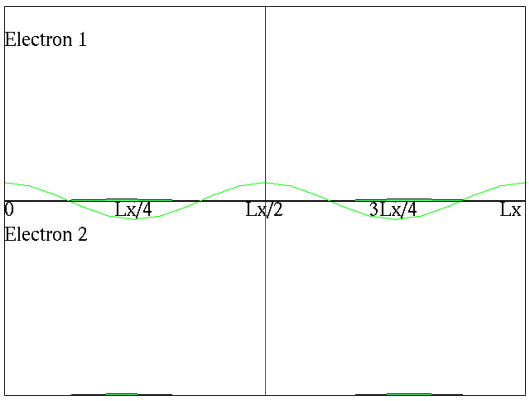

(a) When one is found at the center, the other can be found on both sites.

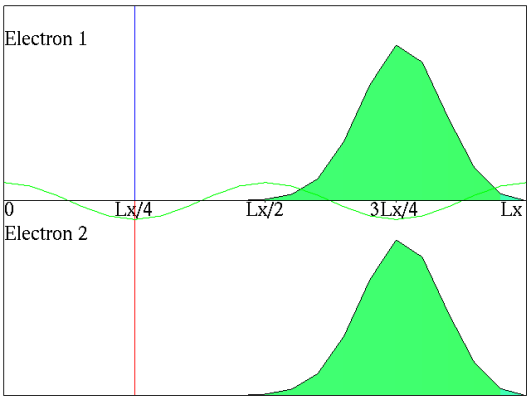

(b) When one is found on the left site, the other can be found on the right sites.

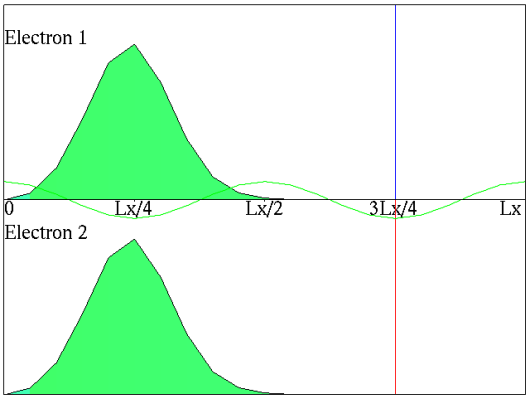

(c) When one is found on the right site, the other can be found on the left sites.

Fig. 4.11: Conditional Probability Density Distribution of a Regime with Hopping and Interaction

After being released from the external confining potential and the lattice potential, the two electrons freely expand and interfere with each other. An "explicit" interference pattern is observed only in Fig. 4.13(a). However, comparing all the figures of Fig. 4.13, it is found that the phase of this state is incoherent. Although each figure has interference maxima, the positions of the maxima differ with each other. When the integral of these patterns are taken, the interference maxima negate each other and the probability density distribution (Fig. 4.12) has no interference pattern left.

This state can be written

$$\begin{aligned} |\Psi\rangle &= \frac{1}{\sqrt{2}}(|LR\rangle + |RL\rangle) \\ &= \frac{1}{2\sqrt{2}}\{(|L\rangle + |R\rangle)_1 \otimes (|L\rangle + |R\rangle)_2 - (|L\rangle - |R\rangle)_1 \otimes (|L\rangle - |R\rangle)_2\}. \end{aligned} \tag{4.36}$$

As an example, let us consider the case where one finds the second indexed electron at the center. According to Eq. (4.36), there are two possible cases $(|L\rangle + |R\rangle)_1 \otimes (|L\rangle + |R\rangle)_2$ and $(|L\rangle - |R\rangle)_1 \otimes (|L\rangle - |R\rangle)_2$. In the latter case, the second indexed electron has a form $(|L\rangle - |R\rangle)$. However, since the left and right sides of the single-electron wave function is joined with the sign "$-$", the interference center is a node and, consequently, the probability density at the center is almost zero. The second indexed electron cannot be found in the latter case and thus the former case is embraced. On the other hand, in the former case, the single-electron wave function of the first indexed electron has the form $(|L\rangle + |R\rangle)$, where the left and right sites are in phase. In this situation, the single-particle interference of the first indexed electron occurs.

Both electrons cannot exist together on a same site. This state can be thought to be a Mott insulator phase. Consequently a Mott insulator phase can be interpreted as being made up with entangled states of the particles.

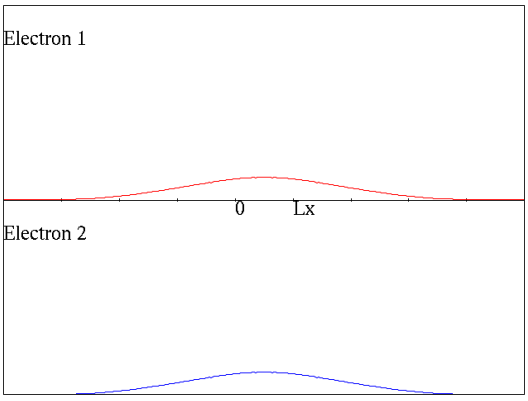

Fig. 4.12: Interference Pattern of a Regime with Hopping and Interaction

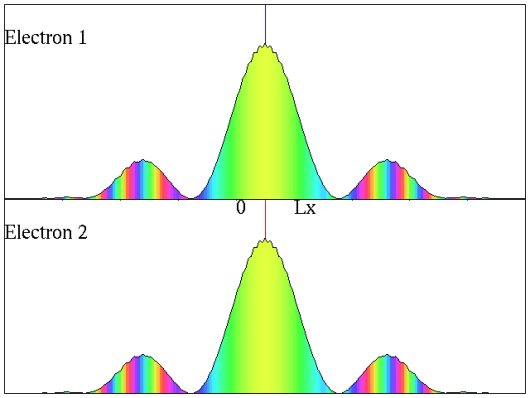

(a) On condition that electron 1 (or 2) is the state $(|L\rangle + |R\rangle)$

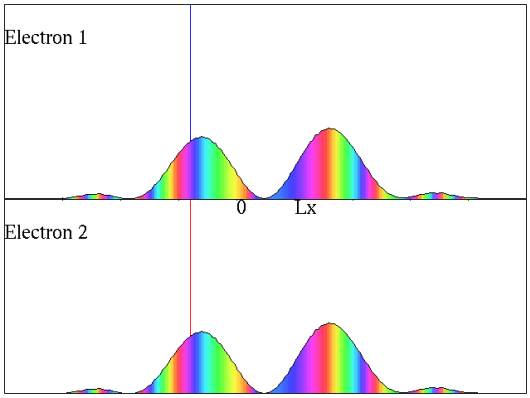

(b) On condition that electron 1 (or 2) is the state $(|L\rangle - |R\rangle)$

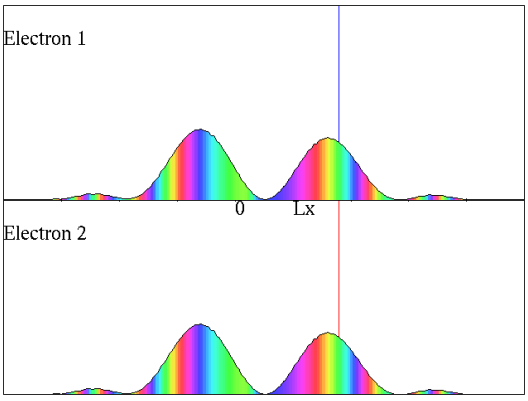

(c) On condition that electron 1 (or 2) is the state $(|L\rangle - |R\rangle)$

Fig. 4.13: Conditional Interference Pattern of a Regime with Hopping and Interaction

Chapter 5

Implementation of FDTD-Q Simulations for a Three-particle System

5.1 Overview

5.1.1 Three-particle Three-site System

In this chapter, the numerical simulation is extended to a three-particle system in a three-site geometry to analyse the property of Mott insulators more generally. Let us consider three particles confined to a plane (see Fig. 5.1). The particles exist within the area:

$$D = \{\, (x, z) \mid 0 < x < L_x,\ 0 < z < L_z \,\} \tag{5.1}$$

in the x-z plane. The external confining potential V_{ext} is described as

$$\begin{cases} V_{\text{ext}} = 0 & (\ (x, z) \in D\ ) \\ V_{\text{ext}} = \infty & (\ \text{else}\ ) \end{cases} . \tag{5.2}$$

The lattice potential V_{lat} is modulated only in x-direction and written

$$V_{\text{lat}}(x, t) = V(t) \cos\left(\frac{6\pi x}{L_x}\right), \tag{5.3}$$

where $V(t) \geq 0$ is the time-transient lattice potential depth.

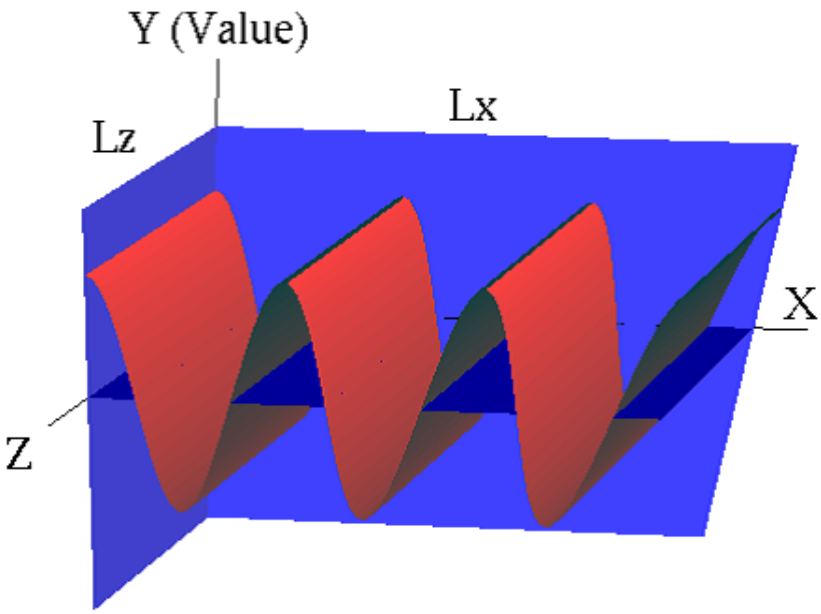

Fig. 5.1: Lattice Potential in the Three-Site Model

5.1.2 Conceptual Expression of the Ground State in the Three-site Model

In this three-site geometry, the ground state of a single particle is simply and conceptually expressed by three basic states $|L\rangle$, $|C\rangle$ and $|R\rangle$, or their superposition state. The $|L\rangle$ state corresponds to a state that the particle is found on the center site ($0 \leq x \leq \frac{L_x}{3}$) and the $|C\rangle$ state corresponds to the center site

($\frac{L_x}{3} \leq x \leq \frac{2L_x}{3}$) and the $|R\rangle$ state corresponds to the right site ($\frac{2L_x}{3} \leq x \leq L_x$). The single-particle ground state of this model written

$$|\Phi\rangle = \frac{1}{\sqrt{3}}(|L\rangle + |C\rangle + |R\rangle). \tag{5.4}$$

The three-particle ground state without any interaction is then written

$$|\Psi\rangle_{U=0} = \frac{1}{\sqrt{3}}(|L\rangle + |C\rangle + |R\rangle)_1 \otimes \frac{1}{\sqrt{3}}(|L\rangle + |C\rangle + |R\rangle)_2 \otimes \frac{1}{\sqrt{3}}(|L\rangle + |C\rangle + |R\rangle)_3. \tag{5.5}$$

Using this expression, we may guess that the ground state of this three-particle system with interactions will be given by

$$|\Psi\rangle_{U\neq 0} = \frac{1}{\sqrt{6}}(|LCR\rangle + |LRC\rangle + |CLR\rangle + |CRL\rangle + |RCL\rangle + |RLC\rangle) \tag{5.6}$$

since interaction energy evokes excitation if two or more particles exist on a same site.

5.2 Implementation

5.2.1 Hamiltonian

Let us consider the situation of three particles confined in the x-z plane, where an external potential is modulated only in x-direction. Eq. (4.11) is then rewritten

$$\begin{aligned}\hat{H}_{3-\mathrm{body}} &= -\frac{\hbar^2}{2m_1}\left(\frac{\partial^2}{\partial x_1^2} + \frac{\partial^2}{\partial z_1^2}\right) - \frac{\hbar^2}{2m_2}\left(\frac{\partial^2}{\partial x_2^2} + \frac{\partial^2}{\partial z_2^2}\right) - \frac{\hbar^2}{2m_3}\left(\frac{\partial^2}{\partial x_3^2} + \frac{\partial^2}{\partial z_3^2}\right) \\ &\quad + V_1(x_1,t) + V_2(x_2,t) + V_3(x_3,t) \\ &\quad + V_{1,2}(x_1,z_1,x_2,z_2) + V_{2,3}(x_2,z_2,x_3,z_3) + V_{3,1}(x_3,z_3,x_1,z_1).\end{aligned} \tag{5.7}$$

In addition, Eq. (4.12) is rewritten

$$\hat{H}_{3-\mathrm{body}}\Psi(x_1,z_1,x_2,z_2,x_3,z_3,t) = i\hbar\frac{\partial}{\partial t}\Psi(x_1,z_1,x_2,z_2,x_3,z_3,t). \tag{5.8}$$

In the following, for simplicity, I assume that the three particles have a same mass and they are spin less bosons. (Note that one can also consider a fermion case if assumes antisymmetrized spin part of the wave function such that the energy is minimized.)

5.2.2 Probability Density

The probability density that the first-labeled particle is found at (x_1, z_1) and the second-labeled particle is found at (x_2, z_2) and the third-labeled particle is found at (x_3, z_3) at a same time t is given by

$$P(x_1,z_1,x_2,z_2,x_3,z_3,t) = |\Psi(x_1,z_1,x_2,z_2,x_3,z_3,t)|^2. \tag{5.9}$$

The x-directional distribution of the probability density of the first-labeled particle is then written

$$P(x_1,t) = \int\int\int\int\int P(x_1,z_1,x_2,z_2,x_3,z_3,t)dz_1dx_2dz_2dx_3dz_3. \tag{5.10}$$

5.2.3 Discretization (Real time)

To calculate the wave function, it must be separated into real and imaginary parts and discretized as described in Sec. 3.2. In the following, I abbreviate the position indexes, that is $R^n_{i_1,j_1,i_2,j_2,i_3,j_3}$ to R^n and $I^n_{i_1,j_1,i_2,j_2,i_3,j_3}$ to I^n. By the same token, for example, $R^n_{i_1+1,j_1,i_2,j_2,i_3,j_3}$ is abbreviated to $R^n_{i_1+1}$. Let us then define the second order differences as the following equations:

$$DiffXR^n = \frac{R^n_{i_1+1} + R^n_{i_1-1} + R^n_{i_2+1} + R^n_{i_2-1} + R^n_{i_3+1} + R^n_{i_3-1} - 6R^n}{(\Delta x)^2} \tag{5.11}$$

$$DiffZR^n = \frac{R^n_{j_1+1} + R^n_{j_1-1} + R^n_{j_2+1} + R^n_{j_2-1} + R^n_{j_3+1} + R^n_{j_3-1} - 6R^n}{(\Delta x)^2} \tag{5.12}$$

$$DiffXI^n = \frac{I^n_{i_1+1} + I^n_{i_1-1} + I^n_{i_2+1} + I^n_{i_2-1} + I^n_{i_3+1} + I^n_{i_3-1} - 6I^n}{(\Delta x)^2} \tag{5.13}$$

$$DiffZI^n = \frac{I^n_{j_1+1} + I^n_{j_1-1} + I^n_{j_2+1} + I^n_{j_2-1} + I^n_{j_3+1} + I^n_{j_3-1} - 6I^n}{(\Delta x)^2}, \tag{5.14}$$

with cell size $\Delta x = \frac{L_x}{N_x}$, $\Delta z = \frac{L_z}{N_z}$. Using this definition the Schrödinger equation is transformed into the following two difference equations:

$$\begin{aligned} R^{n+\frac{1}{2}} &= R^{n-\frac{1}{2}} - \frac{\hbar\Delta t}{2m^*_{\mathrm{e}}}\Big\{DiffXI^n + DiffZI^n\Big\} \\ &\quad + \frac{\Delta t}{\hbar}\Big\{V^n_{i_1} + V^n_{i_2} + V^n_{i_3} + V_{1,2} + V_{2,3} + V_{3,1}\Big\}I^n \end{aligned} \tag{5.15}$$

$$\begin{aligned} I^{n+\frac{1}{2}} &= I^{n-\frac{1}{2}} + \frac{\hbar\Delta t}{2m^*_{\mathrm{e}}}\Big\{DiffXR^n + DiffZR^n\Big\} \\ &\quad - \frac{\Delta t}{\hbar}\Big\{V^n_{i_1} + V^n_{i_2} + V^n_{i_3} + V_{1,2} + V_{2,3} + V_{3,1}\Big\}R^n \end{aligned} \tag{5.16}$$

where $V_{m,n} = V_{\mathrm{int}}\frac{1}{\sqrt{(i_m-i_n)^2(\Delta x)^2+(j_m-j_n)^2(\Delta z)^2}}$ with $\{m,n\} \in \{1,2,3\}$.

In this implementation, I employed the parameters described in Tab. 5.1:

Tab. 5.1: Parameters for the Simulation of a Three-particle System

Name	Symbol	Value	Unit
Width	L_x	3.0×10^{-7}	m
Depth	L_z	1.0×10^{-7}	m
Cell Number for x-direction	N_x	18	–
Cell Number for z-direction	N_z	4	–
Time Step	Δt	1.0×10^{-15}	s

5.2.4 Discretization (Imaginary Time)

Using Eqs. (5.11)-(5.14), the imaginary time evolution is formulated in a similar way to Chap. 4.

$$R^{n+\frac{1}{2}} = R^{n-\frac{1}{2}} + \frac{\hbar\Delta t}{2m^*_{\mathrm{e}}}\Big\{DiffXR^n + DiffZR^n\Big\}$$

$$-\frac{\Delta t}{\hbar}\Big\{V_{i_1}^n + V_{i_2}^n + V_{i_3}^n + V_{1,2} + V_{2,3} + V_{3,1}\Big\}R^n \tag{5.17}$$

$$I^{n+\frac{1}{2}} = I^{n-\frac{1}{2}} + \frac{\hbar\Delta t}{2m_{\mathrm{e}}^*}\Big\{DiffXI^n + DiffZI^n\Big\} - \frac{\Delta t}{\hbar}\Big\{V_{i_1}^n + V_{i_2}^n + V_{i_3}^n + V_{1,2} + V_{2,3} + V_{3,1}\Big\}I^n \tag{5.18}$$

5.3 Experimental Procedure

5.3.1 Initial State

Without any lattice potential and any interaction, the single-electron wave function of the ground state is given by

$$\phi_i(x_i, z_i) = \frac{2}{\sqrt{L_x L_z}} \sin\left(\frac{\pi x_i}{L_x}\right) \sin\left(\frac{\pi z_i}{L_z}\right), \tag{5.19}$$

and the ground-state energy of a single electron is given by

$$E_{\mathrm{GS}} = \frac{\pi^2\hbar^2}{2m_{\mathrm{e}}^*}\left(\frac{1}{{L_x}^2} + \frac{1}{{L_z}^2}\right). \tag{5.20}$$

The wave function of the system is then written

$$\begin{aligned}\Phi(x_1, z_1, x_2, z_2, x_3, z_3) &= \phi_1(x_1, z_1)\phi_2(x_2, z_2)\phi_2(x_3, z_3) \\ &= \left(\frac{2}{\sqrt{L_x L_z}}\right)^3 \prod_{n=1}^{3} \sin\left(\frac{\pi x_n}{L_x}\right) \sin\left(\frac{\pi z_n}{L_z}\right).\end{aligned} \tag{5.21}$$

Following the description in Sec. 3.2, one obtains the following discretized initial values:

$$R^0 = \left(\frac{2}{\sqrt{L_x L_z}}\right)^3 \prod_{n=1}^{3} \sin\left(\frac{\pi i_n}{N_x}\right) \sin\left(\frac{\pi j_n}{N_z}\right) \tag{5.22}$$

$$I^{\frac{1}{2}} = -R^0 \sin\left(\frac{3E_{\mathrm{GS}}\Delta t}{2\hbar}\right). \tag{5.23}$$

5.3.2 Increasing the Lattice Potential

As the lattice potential is gradually increased, without any interactions, the three particles start to localize on each lattice site. Finally, each particle is left in a superposition state of the left, center, and right on-site states. In this state, the particle can tunnel from one site to another. The wave function of the system has the form of Eq. (5.5).

In this simulation, the lattice potential was increased with a step $\Delta V = 2.0 \times 10^{-26}$[J] in half a step ($\frac{\Delta t}{2}$). This was continued from $t = 0$ to $t = 10^3\Delta t$.

5.3.3 Increasing of Both the Interaction Term and the Lattice Potential

After switching on the interaction term at $t = 0$, an imaginary time evolution is performed for an sufficiently long time to calculate the ground state of the interacting system. As the lattice potential is then gradually increased in real time, the particles start to localize on a site.

In this simulation, the imaginary time evolution was iterated for 10^3 steps. After this, the lattice potential was increased with a step $\Delta V = 2.0 \times 10^{-26}$[J] for half a step ($\frac{\Delta t}{2}$). This was continued from $t = 10^3 \Delta t$ to $t = 2 \times 10^3 \Delta t$.

5.3.4 Free Expansion

Released from all potentials after the time evolution, the particles scatter freely and interfere with each other. In this scattering process, only the propagation along the x-axis was calculated since the particles do not interfere as much along the z-direction due to the x-directional site alignment. Furthermore, in this process, the interaction term is set to zero again because it no longer affects the correlation between the three particles after localization.

5.4 Results and Speculations

In this section, there are two types of result figures. One shows probability density distributions of the first indexed particle. The other shows conditional probability density distributions of the first indexed particle on condition that the second indexed particle is found at a red-lined position and the third indexed particle is found at blue-lined position. The inner color indicates a relative phase. In both types of figure, the green line graph indicates the shape of the lattice potential.

5.4.1 Regime with Hopping

After the lattice potential is increased, the particles localize on every three sites with equal phase (see Figs. 5.2 and 5.3). Fig. 5.3 shows that the left, center, and right sides of a single-particle wave function are in phase in this state.

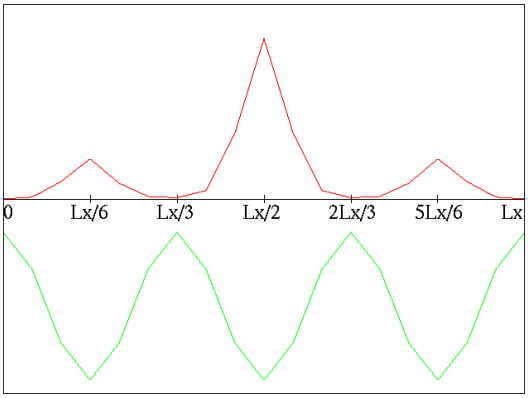

Fig. 5.2: Probability Density Distribution of a Regime with Hopping

After being released from the external confining potential and the lattice potential, the three particles freely expand and interfere with each other. In Figs. 5.4 and 5.5, higher-order maxima are visible. Furthermore Fig. 5.5 show that the interference maxima are always visible wherever the other particles are

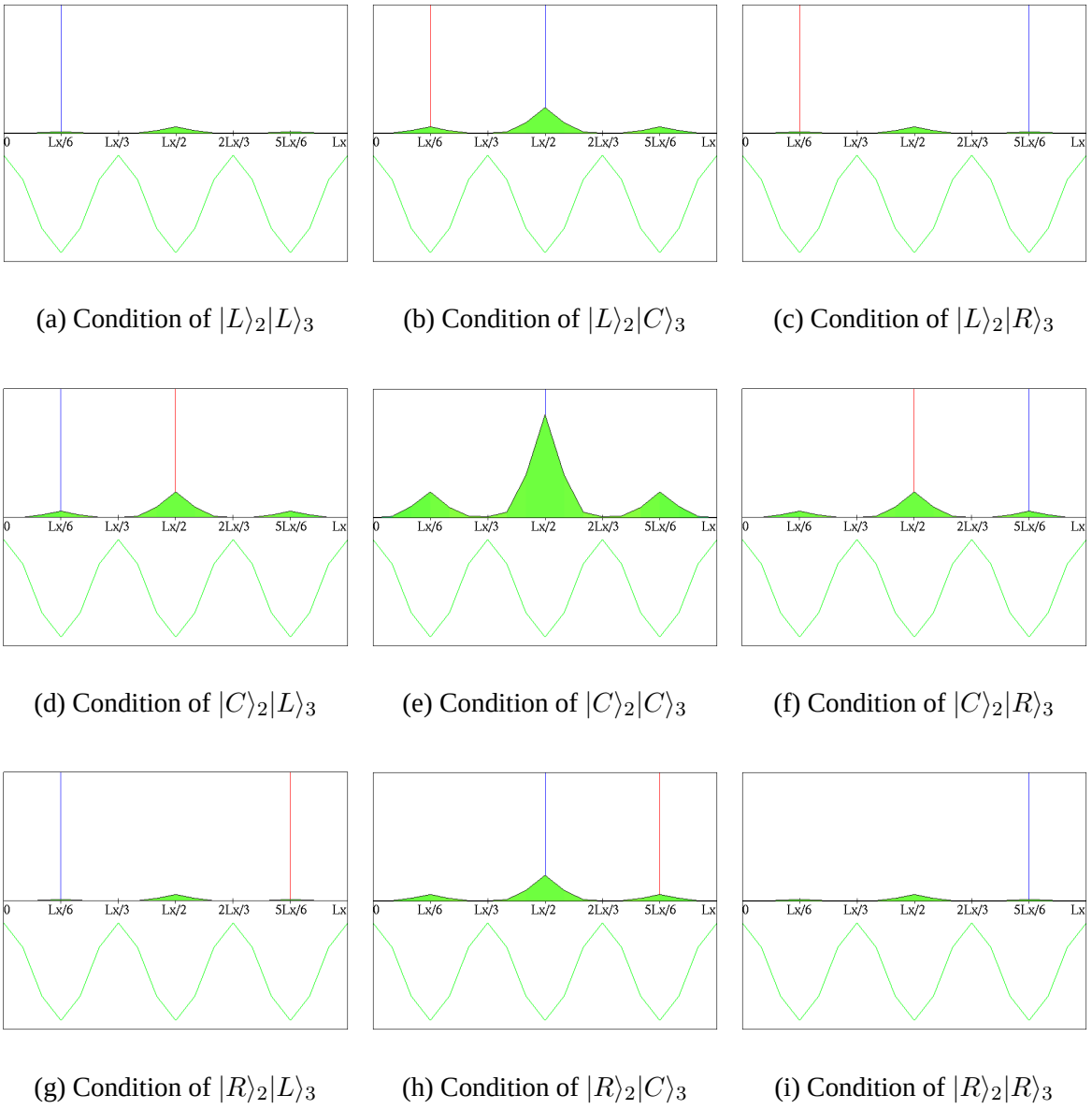

(a) Condition of $|L\rangle_2|L\rangle_3$ (b) Condition of $|L\rangle_2|C\rangle_3$ (c) Condition of $|L\rangle_2|R\rangle_3$

(d) Condition of $|C\rangle_2|L\rangle_3$ (e) Condition of $|C\rangle_2|C\rangle_3$ (f) Condition of $|C\rangle_2|R\rangle_3$

(g) Condition of $|R\rangle_2|L\rangle_3$ (h) Condition of $|R\rangle_2|C\rangle_3$ (i) Condition of $|R\rangle_2|R\rangle_3$

Fig. 5.3: Conditional Probability Density Distribution of a Regime with Hopping

found. Consequently, the sum of these phenomena also shows an interference maxima in the probability density distribution (Fig. 5.4).

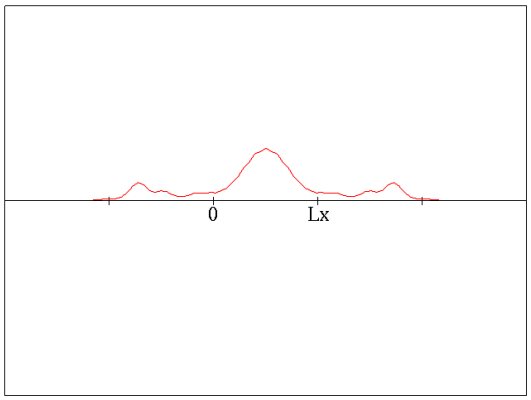

Fig. 5.4: Interference Pattern of a Regime with Hopping

This state can be written

$$|\Psi\rangle = \frac{1}{2}(|L\rangle + |C\rangle + |R\rangle)_1 \otimes (|L\rangle + |C\rangle + |R\rangle)_2 \otimes (|L\rangle + |C\rangle + |R\rangle)_3. \tag{5.24}$$

All particles can hop from one site to another site respectively. This phase consists of quantum superposition states of each particle and, consequently, can be thought to be a superfluid phase.

5.4.2 Regime with Hopping and Interaction

After the imaginary time evolution and the increase of the lattice potential, the particles begin localizing on an individual site (see Figs. 5.6 and 5.7). This state has a correlation between the positions of the particles. That is to say, if one particle is found on one site and another particle is found on another site, the last particle can then be found on the last site.

After being released from the external confining potential and the lattice potential, the three particles freely expand and interfere with each other. An “explicit” interference pattern is observed only in Fig. 5.9(a). However, comparing each of the figures in Fig. 5.9, one can see that the phase of this state is incoherent. Although each figure has interference maxima, the positions of the maxima differ with each other. When the integral of these phenomena is taken, the interference maxima negate each other and the probability density distribution (Fig. 5.8) has no interference pattern left.

This state can be represented by Eq. (5.6). In this situation, the single-particle interference maxima of one particle exist at different positions which depend on the positions of other particles.

Either particle cannot exist together on the same site. This state can be thought to be a Mott insulator state. Consequently a Mott insulator quantum can be interpreted to be made up of entangled states of the particles.

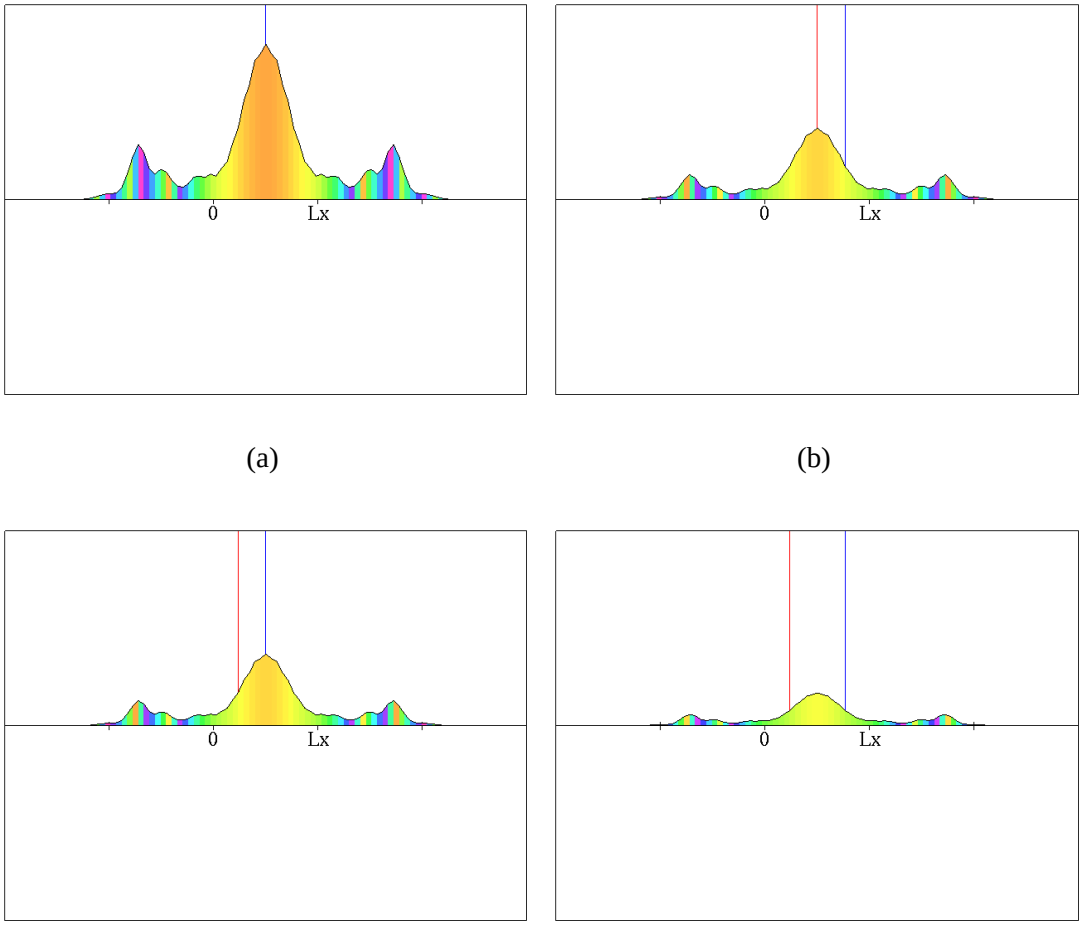

Fig. 5.5: Conditional Interference Pattern of a Regime with Hopping

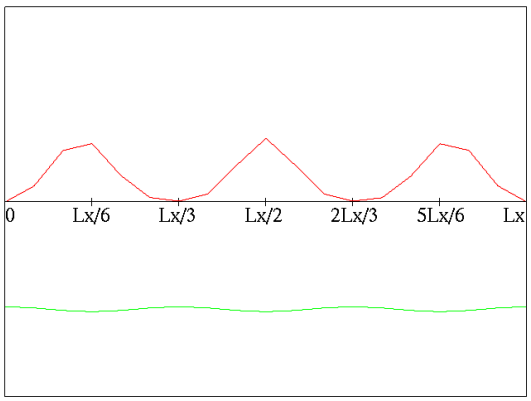

Fig. 5.6: Probability Density Distribution of a Regime with Hopping and Interaction

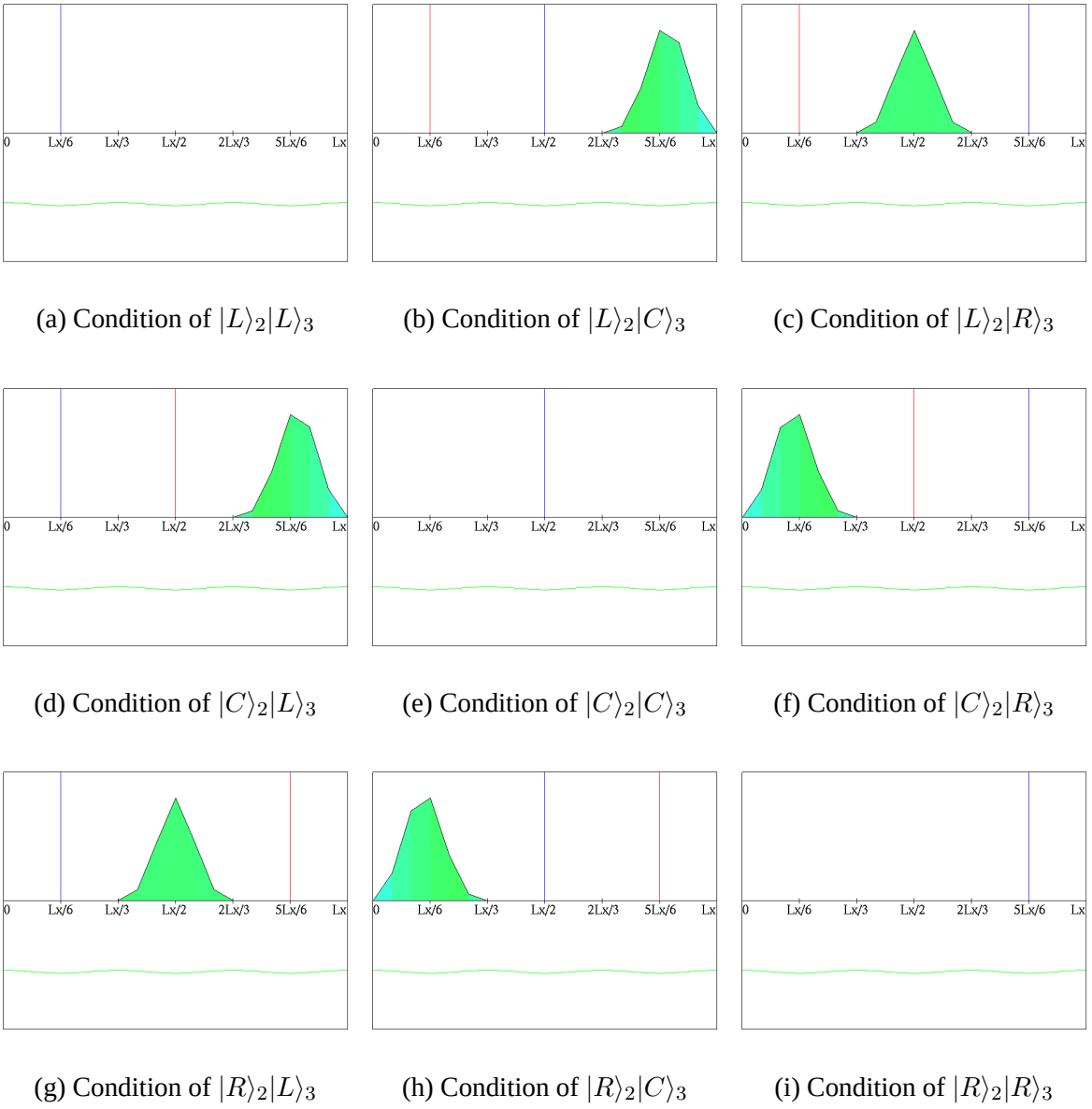

(a) Condition of $|L\rangle_2|L\rangle_3$ (b) Condition of $|L\rangle_2|C\rangle_3$ (c) Condition of $|L\rangle_2|R\rangle_3$

(d) Condition of $|C\rangle_2|L\rangle_3$ (e) Condition of $|C\rangle_2|C\rangle_3$ (f) Condition of $|C\rangle_2|R\rangle_3$

(g) Condition of $|R\rangle_2|L\rangle_3$ (h) Condition of $|R\rangle_2|C\rangle_3$ (i) Condition of $|R\rangle_2|R\rangle_3$

Fig. 5.7: Conditional Probability Density Distribution of a Regime with Hopping and Interaction

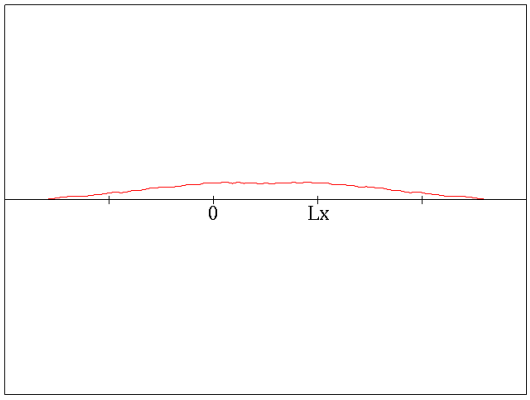

Fig. 5.8: Interference Pattern of a Regime with Hopping and Interaction

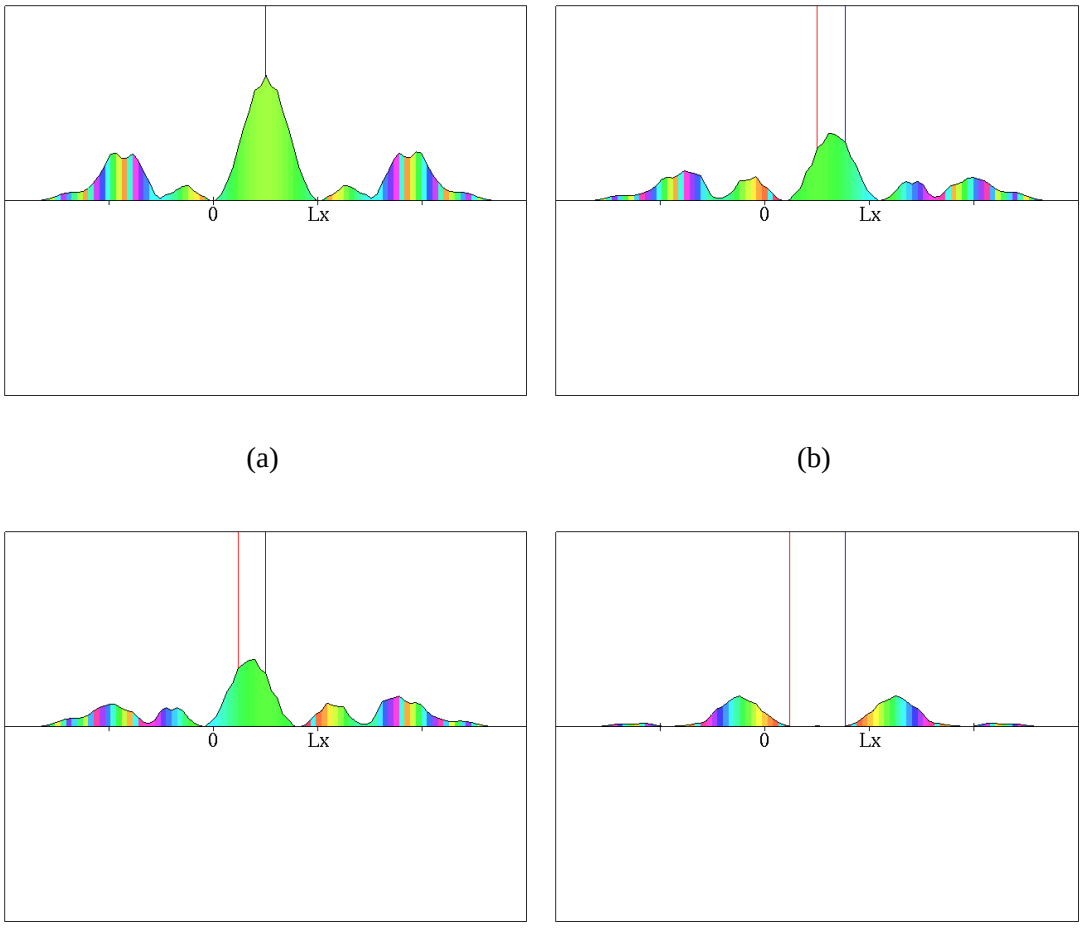

(a) (b)

(c) (d)

Fig. 5.9: Conditional Interference Pattern of a Regime with Hopping

Chapter 6

Conclusions

6.1 Results of This Study

In this study, the wave function of a two-electron system in a two-site geometry was numerically simulated. The Hamiltonian of this system contains both the kinetic energy and the repulsive Coulomb interaction term. The dominant term therefore determines the properties of the system. The ground state of the system was obtained by adiabatic evolution of the parameters. After obtaining the ground state, the system was released from all potentials and interactions and the interference patterns of the probability density distribution was obtained. From analyses of these patterns, two typical quantum phases of the system were confirmed:a metal phase and a Mott insulator phase.

In a metal phase, or a superfluid phase if considering bosons, the left and right sides of a single-electron wave function were in phase for any place. This has the same interference pattern as a single-particle interference pattern. A metal phase is therefore made up with superposition states of each electron as expected.

In a Mott insulator phase, if one electron is found on one site, the other electron is found on the opposite site. Therefore a single-particle interference pattern with maxima at different points which depends on the position of the other particle is observed. Summed up these interference patterns, a probability density distribution that is totally broadened and with interference is obtained. A Mott insulator phase can thus be thought to consist of entangled states of the particles.

6.2 Future Prospects

In this study, I simulated the two typical cases:non-interacting case ($U = 0$) and strongly interacting case. One may also consider points nearer to the cross-over point where the dominant term of the Hamiltonian changes.

In this dissertation, I also considered a three-particle case and obtained similar results to the two-particle case. We may also consider simulations of systems with more particles in order to look at cases near the quantum critical point, as a true phase transition occurs only for an infinite number of particles.

Acknowledgements

First and foremost, I would like to express my deepest gratitude to my supervisor, Professor Yoshihisa Yamamoto for his excellent guidance and kind support. Without his help, I could not have accomplished my work. I also would like to thank Dr. Tim Byrnes for his invaluable comments on the study.

I would like to extend grateful thanks to the members of the Quantum Information Science group at National Institute of Informatics, Research Organization of Information and Systems. Thanks to their continuous aid, my academic life was made possible.

Last but not least, I would like to show my appreciation to my family for their support over the years.

February 2nd, 2007
Fumitaka Fujiwara

References

[1] J. H. de Boer and E. J. W. Verwey: “Semi-conductors with partially and with completely filled $_3d$-lattice bands”, Proceedings of the Physical Society, Vol. 49, No. 4S, pp. 59-71, Aug. 1937.

[2] N. F. Mott and R. Peierls: “Discussion of the paper by de Boer and Verwey”, Proceedings of the Physical Society, Vol. 49, No. 4S, pp. 72-73, Aug. 1937.

[3] N. F. Mott: “The Basis of the Electron Theory of Metals, with Special Reference to the Transition Metals”, Proceedings of the Physical Society, Section A, Vol. 62, No. 7, pp. 416-422, Jul. 1949.

[4] J. Hubbard: “Electron correlations in narrow energy bands”, Proceedings of the Royal Society of London. Series A, Mathematical and Physical Sciences, Vol. 276, No. 1365, pp. 238-257, Nov. 1963.

[5] Elliott H. Lieb: “The Hubbard Model: Some Rigorous Results and Open Problems”, Proceedings of the conference, *Advances in Dynamical Systems and Quantum Physics*, pp. 173-193, May 1993. (Archived as arXiv:cond-mat9311033 v2 15 Nov 1993)

[6] Hal Tasaki: “The Hubbard Model – Introduction and Selected Rigorous Results”, arXiv:cond-mat/9512169v4 19 Dec 1997, Dec. 1997.

[7] Hal Tasaki: “From Nagaoka’s Ferromagnetism to Flat-Band Ferromagnetism and Beyond – An Introduction to Feromagnetism in the Hubbard Model –”, Progress of Theoretical Physics, Vol. 99, No. 4, pp. 489-548, Apr. 1998.

[8] Tôru Moriya and Kazuo Ueda: “Antiferromagnetic spinfluctuation and superconductivity”, Reports on Progress in Physics, Vol. 66, Issue 8, pp. 1299-1341, Aug. 2003.

[9] Matthew P. A. Fisher: “Boson localization and the superfluid-insulator transition”, Physical Review B, Vol. 40, No. 1, pp. 546-570, Jul. 1989.

[10] N. Elstner and H. Monien: “Dynamics and thermodynamics of the Bose-Hubbard model”, Physical Review B, Vol. 59, No. 19, pp. 12184-12187, May 1999.

[11] Fernando M. Cucchietti, Bogdan Damski, Jacek Dziarmaga, and Wojciech H. Zurek: “Dynamics of the Bose-Hubbard model: transition from Mott insulator to superfluid”, arXiv:cond-mat/0601650 v4 16 Oct 2006, Oct. 2006.

[12] D. Jaksch, C. Bruder, J. I. Cirac, C. W. Gardiner, and P. Zoller: “Cold Bosonic Atoms in Optical Lattices”, Physical Review Letters, Vol. 81, No. 15, pp. 3108-3111, Oct. 1998.

[13] Franco Dalfovo, Stefano Giorgini, Lev P. Pitaevskii, and Sandro Stringari: “Theory of Bose-Einstein condensation in trapped gases”, Reviews of Modern Physics, Vol. 71, No. 3, pp. 463-512, Apr. 1999.

[14] Richard P. Feynman: “Simulating Physics with Computers”, International Journal of theoretical Physics, Vol. 21, Nos. 6/7, pp. 467-488, 1982.

[15] Seth Lloyd: “Universal Quantum Simulators”, Science, Vol. 273, No. 5278, pp. 1073-1078, Aug. 1996.

[16] Peter W. Shor: “Algorithms for Quantum Computation: Discrete Logarithms and Factoring”, Proceedings of 35th IEEE FOCS, pp. 124-134, Santa Fe, NM, Nov. 1994.

[17] Markus Greiner, Olaf Mandel, Tilman Esslinger, Theodor W. Hänsch, and Immanuel Bloch: “Quantum phase transition form a superfluid to a Mott insulator in a gas of ultracold atoms”, Nature, Vol. 415, pp. 39-44, Jan. 2002.

[18] Michael Köhl, Henning Moritz, Thilo Stöferle, Kenneth Günter, and Tilman Esslinger: “Fermionic Atoms in a Three Dimensional Optical Lattice: Observing Fermi Surfaces, Dynamics, and Interactions”, Physical Review Letters, Vol. 94, No. 8, Article 080403, Mar. 2005.

[19] Tim Byrnes, Patrik Recher, Na Young Kim, Shoko Utsunomiya, and Yoshihisa Yamamoto: “Quantum simulator for the Hubbard model with long-range Coulomb interactions using surface acoustic waves”, arXiv:cond-mat/0608142 v2 9 Aug 2006, Aug. 2006.

[20] J. M. Shilton, V. I. Talyanskii, M. Pepper, D. A. Ritchie, J. E. F. Frost, C. J. B. Ford, C. G. Smith, and G. A. C. Jones: “High-frequency single-electron tansport in a quasi-one-dimensional GaAs channel induced by surface acoustic waves”, Journal of Physics: Condensed Matter, Vol. 8, Issue 38, pp. L531-L539, Sep. 1996.

[21] Abraham Goldberg, Harry M. Schey, and Judah L. Schwartz: “Computer-Generated Motion Pictures of One-Dimensional Quantum-Mechanical Transmission and Reflection Phenomena”, American Journal of Physics, Vol. 35, No. 3, pp. 177-186, Mar. 1967.

[22] A. Askar and A. S. Cakmak: “Explicit integration method for the time-dependent Schrodinger equation for collision problems”,Journal of Chemical Physics, Vol. 68, No. 6, pp. 2794-2798, Mar. 1978.

[23] Robert L. W. Chen: “Computer graphics for solution of time-dependent Schrödinger equations”, American Journal of Physics, Vol. 50, No. 10, pp. 902-906, Oct. 1982.

[24] M. M. Cerimele, M. L. Chiofalo, Pistella, S. Succi, and M. P. Tosi: “Numerical solution of the Gross-Pitaevskii equation using an explicit finite-difference scheme: An application to trapped Bose-Einstein condensates”, Physical Review E, Vol. 62, No. 1, pp. 1382-1389, Jul. 2000.

[25] Jon. J. V. Maestri, Rubin H. Landau, and Manuel J. Páez: “Two-Particle Schrödinger Equation Animations of Wavepacket-Wavepacket Scattering (revised)”, arXiv:physics/9909042 v1 22 Sep 1999, Jun. 2005.

[26] Kane Yee: “Numerical solution of initial boundary value problems involving maxwell’s equations in isotropic media”, IEEE Transactions on Antennas and Propagation, Vol. 14, Issue 3, pp. 302-307, May 1966.

[27] Allen Taflove and Morris E. Brodwin: “Numerical Solution of Steady-State Electromagnetic Scattering Problems Using the Time-Dependent Maxwell’s Equations”, IEEE Transactions on Microwave Theory and Techniques, Vol. MTT-23, No. 8, pp. 623-630, Aug. 1975.

[28] P. B. Visscher: “A fast explicit algorithm for the time-dependent Schrödniger equation”, Computers in Physics, Vol. 5, Issue 6, pp. 596-598, Nov. 1991.

[29] Antonio Soriano, Enrique A. Navarro, Jorge A. Portí and, Vicente Such: “Analysis of the finite difference time domain technique to solve the Schrödinger equation for quantum devices”, Journal of Applied Physics, Vol. 95, No. 12, pp. 8011-8018, Jun. 2004.

[30] Weizhong Dai, Guang Li, Raja Nassar, and Shengjun Su: “On the Stability of the FDTD Method for Solving a Time-dependent Schrödinger Equation”, Numerical Methods for Partial Differential Equations, Vol. 21, Issue 6, pp. 1140-1154, Nov. 2005.

[31] Tsugumichi Shibata: “Absorbing boundary conditions for the finite-difference time-domain calculation of the one-dimensional Schrödinger equation”, Physical Review B, Vol. 43, No. 8, pp. 6760-6763, Mar. 1991.

[32] J. P. Kuska: “Absorbing boundary conditions for the Schrödinger equation on finite intervals”, Physical Review B, Vol. 46, No. 8, pp. 5000-5003, Mar. 1991.

[33] Zhenli Xu and Houde Han: “Absorbing boundary conditions for nonlinear the Schrödinger equations”, Physical Review E, Vol. 74, No. 037704, Sep. 2006.

[34] Zhenli Xu, Houde Han, and Xiaonan Wu: “Adaptive absorbing boundary conditions for Schrödinger-type equations: application to nonlinear and multi-dimensional problems”, arXiv:math.NA/0610642 v2 3 Nov 2006, Nov. 2006.

[35] Thomas Fevens and Hong Jiang: “Absorbing boundary conditions for the Schrödinger equation”, SIAM Journal on Scientific Computing, Vol. 21, No. 1, pp. 255-282, Sep. 1999.

[36] Nicolae Carjan, Margarit Rizea, and Dan Strottman: “Efficient numerical solution of the time-dependent Schrödinger equation for deep tunneling”, Romanian Reports in Physics, Vol. 55, No. 4, pp. 555-579, 2003.

[37] R. C. Grimm and R. G. Storer: “Monte-Carlo solution of Schrödinger’s equation”, Journal of Computational Physics, Vol. 7, Issue 1, pp. 134-156, Feb. 1971.

[38] Ioan Kosztin, Byron Faber, and Klaus Schulten: “Introduction to the Diffusion Monte Carlo Method”, American Journal of Physics, Vol. 64, Issue 5, pp. 633-644, May 1996.

[39] R. J. Needs, P. R. C. Kent, A. R. Porter, M. D. Towler, and G. Rajagopal: “Quantum Monte Carlo Calculations for Ground and Excited States”, International Journal of Quantum Chemistry, Vol. 86, Issue 2, pp. 218-225, 2002.

[40] R. Grimm and R. G. Storer: “A new method for the numerical solution of the Schrödinger equation”, Journal of Computational Physics, Vol. 4, Issue 2, pp. 230-249, Aug. 1969.

[41] M. L. Chiofalo, S. Succi, and M. P. Tosi: “Ground state of trapped interacting Bose-Einstein condensates by an explicit imaginary-time algorithm”, Physical Review E, Vol. 62, No. 5, pp. 7438-7444, Nov. 2000.

Appendix A

Constants

Tab. A.1: Physical Constants

Name	Symbol	Value	Unit
Permittivity of free space	ε_0	$8.854187817 \times 10^{-12}$	$\mathrm{F \cdot m^{-1}}$
Planck's constant	h	6.62607×10^{-34}	$\mathrm{J \cdot s}$
Dirac's constant	$\hbar = \frac{h}{2\pi}$	1.054572×10^{-34}	$\mathrm{J \cdot s}$
Elementary charge	e	1.602177×10^{-19}	C
Electron rest mass	m_e	9.10938×10^{-31}	kg
Relative permittivity in GaAs	ε_r	1.31×10^{1}	-
Electron effective mass in GaAs	m_e^*	$0.067 m_\mathrm{e}$	kg
Circle ratio (C/C++ compiler definition)	π	3.14159265358979323846	-

Appendix B

HSV Color Space

The HSV (Hue, Saturation, Value) model is a nonlinear transformation of the RGB color space. It defines a color space in terms of three components:

- Hue, the color type
  Ranges from 0 to 360 ˚.
- Saturation (Purity), the vibrancy of the color
  Ranges from 0 to 100%.
- Value, the brightness of the color
  Ranges from 0 to 100%.

The definition of the HSV color model is device-dependent. HSV is only defined relative to RGB intensities without the physical definitions of chromaticities and white point. This model may be used in color progressions.

Transformations between RGB and HSV

The ranges of the values:

$$\begin{aligned} H &\in (0, 360) \\ S, V, R, G, B &\in (0, 1) \end{aligned}$$

- From RGB to HSV
  Let MAX equal the maximum of the (R, G, B) values, and MIN equal the minimum of those values.

$$H = \begin{cases} \text{undefined}, & \text{if} \quad MAX = MIN \\ 60 \times \frac{G-B}{MAX-MIN}, & \text{if} \quad MAX = R \quad \text{and} \quad G \geq B \\ 60 \times \frac{G-B}{MAX-MIN} + 360, & \text{if} \quad MAX = R \quad \text{and} \quad G < B \\ 60 \times \frac{B-R}{MAX-MIN} + 120, & \text{if} \quad MAX = G \\ 60 \times \frac{R-G}{MAX-MIN} + 240, & \text{if} \quad MAX = B \end{cases} \tag{B.1}$$

$$S = \begin{cases} 0, & \text{if} \quad MAX = 0 \\ 1 - \frac{MIN}{MAX}, & \text{else} \end{cases} \tag{B.2}$$

$$V = MAX \tag{B.3}$$

- From HSV to RGB

$$\begin{cases} H_i &= \left\lfloor \frac{H}{60} \right\rfloor \mod 6 \\ f &= \frac{H}{60} - H_i \\ p &= V(1 - S) \\ q &= V(1 - fS) \\ t &= V(1 - (1 - f)S) \end{cases}$$

$$\begin{cases} R = V, & G = t, & B = p, & \text{if} & H_i = 0 \\ R = q, & G = V, & B = p, & \text{if} & H_i = 1 \\ R = p, & G = V, & B = t, & \text{if} & H_i = 2 \\ R = p, & G = q, & B = V, & \text{if} & H_i = 3 \\ R = t, & G = p, & B = V, & \text{if} & H_i = 4 \\ R = V, & G = p, & B = q, & \text{if} & H_i = 5 \end{cases} \tag{B.4}$$

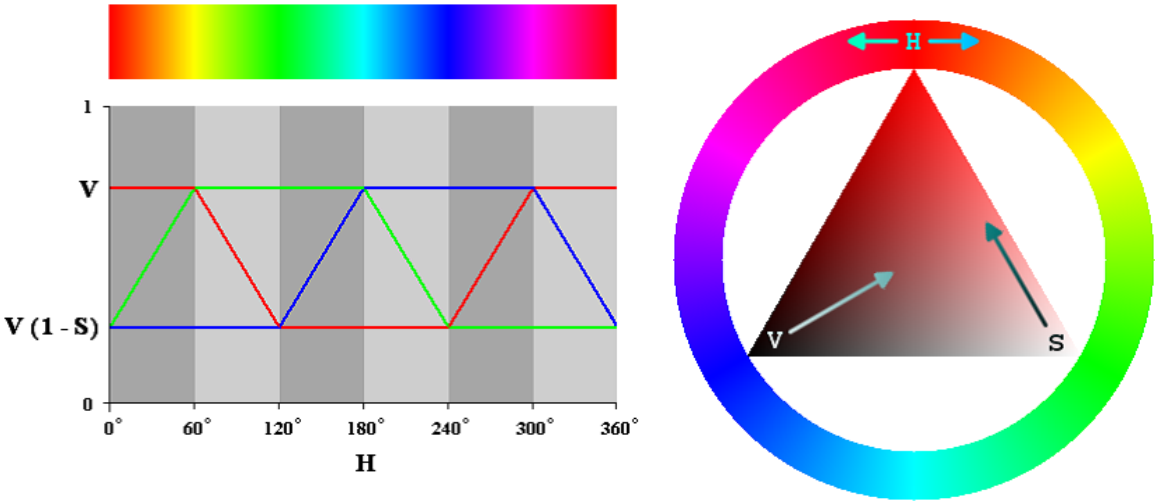

(a) Relationship between HSV and RGB (b) HSV Color Wheel

Fig. B.1: HSV Color Space